RESEARCH

Turbulence Effects on the Statistical Behaviour and Modelling of Flame Surface Density and the Terms of Its Transport Equation in Turbulent Premixed Flames

Arun Ravi Varma[1] · Umair Ahmed[1] · Nilanjan Chakraborty[1]

Abstract

The influence of the ratio of integral length scale to flame thickness on the statistical behaviours of flame surface density (FSD) and its transport has been analysed using a Direct Numerical Simulation database of three-dimensional statistically planar turbulent premixed flames for different turbulence intensities. It has been found that turbulent burning velocity based on volume-integration of reaction rate and flame surface area increase but the peak magnitudes of the FSD and the terms of the FSD transport term decrease with an increase in length scale ratio for a given turbulence intensity. The flame brush thickness and flame wrinkling increase with an increase in length scale ratio for all turbulence intensities. However, the qualitative behaviours of the unclosed terms in the FSD transport equation remain unaltered by the length scale ratio and in all cases the tangential strain rate term and the curvature term act as leading order source and sink, respectively. A decrease in length scale ratio for a given turbulence intensity leads to a decrease in Damköhler number and an increase in Karlovitz number. This has an implication on the alignment of reactive scalar gradient with local strain rate eigenvectors, which in turn increases positive contribution of the tangential strain rate term with a decrease in length scale ratio. Moreover, an increase in Karlovitz number increases the likelihood of negative contribution of the curvature term. Thus, the magnitude of the negative contribution of the FSD curvature term increases with a decrease in length scale ratio for a given turbulence intensity. The model for the tangential strain rate term, which explicitly considers the scalar gradient alignment with local principal strain rate eigenvectors, has been shown to be more successful than the models that do not account for the scalar gradient alignment characteristics. Moreover, the existing model for the curvature and propagation term needed modification to account for greater likelihood of negative values for higher Karlovitz number. However, the models for the unclosed flux of FSD and the mean reaction rate closure are not significantly affected by the length scale ratio.

Keywords Flame surface density · Length scale ratio · Turbulence intensity · Mean reaction rate closure · Direct numerical simulations

✉ Nilanjan Chakraborty
nilanjan.chakraborty@ncl.ac.uk

[1] School of Engineering, Newcastle University, Claremont Road, Newcastle Upon-Tyne NE1 7RU, UK

1 Introduction

The non-linear temperature and species mass fraction dependences of the chemical reaction rate make the closure of mean reaction rate a challenging task in the modelling of turbulent reacting flows. One of the ways that this challenge can be bypassed in turbulent premixed combustion modelling is the closure of flame surface area to volume ratio (Pope 1988; Candel and Poinsot 1990) according to the Flame Surface Density (FSD) based methodology (Pope 1988; Candel and Poinsot 1990; Poinsot and Veynante 2001) under flamelet assumption, which assumes that the consumption rate of reactants per unit flame surface area remains identical to that for the laminar flame. However, the FSD is an unclosed quantity and several attempts have been made to model this quantity based on algebraic (Bray 1980; Cant and Bray 1988, 1989; Abu-Orf and Cant 2000; Boger et al. 1998; Charlette et al. 2002; Knikker et al. 2002; Fureby 2005; Chakraborty and Klein 2008; Ma et al. 2013; Keppeler et al. 2014; Klein et al. 2016; Ahmed et al. 2021; Rasool et al. 2022) and transport equation (Cant et al. 1990; Candel et al. 1990; Duclos et al. 1993; Trouvé and Poinsot 1994; Veynante et al. 1996; Hawkes and Cant 2000, 2001; Chakraborty and Cant 2007, 2009a, 2011, 2013; Hun and Huh 2008; Hernandez-Perez et al. 2011; Katragadda et al. 2011, 2014a, b; Reddy and Abraham 2012; Ma et al. 2014; Sellmann et al. 2017; Papapostolou et al. 2019; Luca et al. 2019; Keil et al. 2020; Varma et al. 2022a; Berger et al. 2022) closures in the context of Reynolds Averaged Navier–Stokes (RANS) (Bray 1980; Cant and Bray 1988, 1989; Cant et al. 1990; Candel et al. 1990; Duclos et al. 1993; Trouvé and Poinsot 1994; Veynante et al. 1996; Abu-Orf and Cant 2000; Hun and Huh 2008; Chakraborty and Cant 2011, 2013; Ahmed et al. 2021; Katragadda et al. 2011, 2014b; Sellmann et al. 2017; Papapostolou et al. 2019; Luca et al. 2019; Rasool et al. 2022; Varma et al. 2022a; Berger et al. 2022) and Large Eddy Simulations (LES) (Boger et al. 1998; Charlette et al. 2002; Knikker et al. 2002; Fureby 2005; Chakraborty and Klein 2008; Chakraborty and Cant 2007, 2009a; Hun and Huh 2008; Hernandez-Perez et al. 2011; Reddy and Abraham 2012; Ma et al. 2013, 2014; Katragadda et al. 2014a; Keppeler et al. 2014; Klein et al. 2016; Keil et al. 2020). The algebraic closures are designed for the situations where an equilibrium is maintained between the generation and destruction rates of flame surface area (Bray 1980; Cant and Bray 1988, 1989; Abu-Orf and Cant 2000; Boger et al. 1998; Charlette et al. 2002; Knikker et al. 2002; Fureby 2005; Chakraborty and Klein 2008; Ma et al. 2013; Keppeler et al. 2014; Klein et al. 2016; Ahmed et al. 2021; Rasool et al. 2022). However, this equilibrium may not be maintained in flame instabilities and under this condition a modelled transport equation for the FSD might be necessary (Cant et al. 1990; Candel et al. 1990; Duclos et al. 1993; Trouvé and Poinsot 1994; Veynante et al. 1996; Hawkes and Cant 2000, 2001; Chakraborty and Cant 2007, 2009a, 2011, 2013; Hun and Huh 2008; Hernandez-Perez et al. 2011; Katragadda et al. 2011, 2014a, b; Reddy and Abraham 2012; Ma et al. 2014; Sellmann et al. 2017; Papapostolou et al. 2019; Luca et al. 2019; Keil et al. 2020; Varma et al. 2022a; Berger et al. 2022). The advancements of computational power have enabled significant improvements in the FSD modelling using Direct Numerical Simulations (DNS) data (Trouvé and Poinsot 1994; Boger et al. 1998; Charlette et al. 2002; Chakraborty and Cant 2007, 2009a, 2011, 2013; Hun and Huh 2008; Chakraborty and Klein 2008; Katragadda et al. 2011, 2014a, b; Reddy and Abraham 2012; Klein et al. 2016; Ahmed et al. 2021; Rasool et al. 2022; Papapostolou et al. 2019; Luca et al. 2019; Keil et al. 2020; Varma et al. 2022a; Berger et al. 2022). Among these studies, there have been analyses where the effects of Lewis number (Trouvé and Poinsot 1994; Hun and Huh 2008; Chakraborty and Cant 2011; Katragadda et al. 2011, 2014a, b; Berger et al. 2022), turbulent Reynolds number (Chakraborty and Cant 2013; Luca et al. 2019), buoyancy (or Froude number) (Varma

et al. 2022a) and thermodynamic pressure (Keil et al. 2020) on the statistical behaviour of the FSD and its transport were addressed. A number of recent experimental (Kim et al., 2022) and computational (Yu et al. 2017; Varma et al. 2022a; Song et al. 2021, 2022; Trivedi et al. 2022) analyses revealed that the flame surface area and turbulent burning velocity for a given turbulence intensity increase with an increase in integral length scale to flame thickness ratio. Moreover, the analysis by Varma et al. (2022a) further demonstrated that the volume integrated values of the strain rate and curvature contributions to the FSD transport increase with increasing integral length scale to flame thickness ratio. Thus, it is expected that the ratio of integral length scale to flame thickness is likely to have an influence on the statistical behaviours of the FSD and the terms of its transport equation. However, to date, the effects of integral length scale to flame thickness ratio on the statistical behaviour of the FSD and the terms of its transport equation for different turbulence intensities are yet to be analysed in detail. This gap in the existing literature has been addressed in this paper and in this respect, the main objectives of this paper are: (a) to demonstrate the effects of the length scale separation on the magnitudes and statistical behaviours of FSD, wrinkling factor and the unclosed terms of the FSD transport equation, and (b) to indicate modelling implications of the different values of turbulence intensity and length scale ratio on the closure of different terms of the FSD transport equation and identify the appropriate model expressions.

The rest of the paper will be organised in the following manner. The mathematical background and numerical implementation relevant to this analysis are presented in Sects. 2 and 3, respectively. This will be followed by the presentation of results and their discussion. The main findings of the present analysis are summarised, and conclusions are drawn in Sect. 5.

2 Mathematical Background

The reactive scalar field in premixed combustion is often represented by reaction progress variable c, which can be defined based on a suitable species α mass fraction Y_α in the following manner:

$$c = (Y_\alpha - Y_{\alpha,R})/(Y_{\alpha,P} - Y_{\alpha,R}) \tag{1}$$

where subscripts R and P represent values in the fully unburned reactants and fully burned products, respectively. According to Eq. (1) c increases from 0 from the unburned reactants to 1.0 in the fully burned products. The transport equation for c takes the following form:

$$\frac{\partial(\rho c)}{\partial t} + \frac{\partial(\rho u_j c)}{\partial x_j} = \frac{\partial}{\partial x_j}\left(\rho D \frac{\partial c}{\partial x_j}\right) + \dot{\omega} \tag{2}$$

where u_j is the jth component of velocity, ρ is density, D is the reaction progress variable diffusivity and $\dot{\omega} = \dot{\omega}_\alpha/(Y_{\alpha,P} - Y_{\alpha,R})$ is the reaction rate of the progress variable with $\dot{\omega}_\alpha$ being the reaction rate of species α. On Reynolds averaging Eq. (2) one obtains:

$$\frac{\partial(\overline{\rho}\tilde{c})}{\partial t} + \frac{\partial(\overline{\rho}\tilde{u}_j\tilde{c})}{\partial x_j} = \overline{\frac{\partial}{\partial x_j}\left(\rho D \frac{\partial c}{\partial x_j}\right)} + \overline{\dot{\omega}} - \frac{\partial\overline{(\rho u_j'' c'')}}{\partial x_j} \tag{3}$$

where $\overline{q}, \tilde{q} = \overline{\rho q}/\overline{\rho}$ and $q'' = q - \tilde{q}$ are the Reynolds averaged, Favre averaged and Favre fluctuations of a general quantity q, respectively. All the terms on the right-hand side of Eq. (3) are unclosed and need modelling. The closure of the last term needs modelling of

turbulent scalar flux $\overline{(\rho u_j'' c'')}$ and the first two terms are modelled in the following manner in the context of FSD based methodology (Trouvé and Poinsot 1994; Boger et al. 1998):

$$\overline{\nabla \cdot (\rho D \nabla c)} + \overline{\dot{\omega}} = \overline{(\rho S_d)}_s \Sigma_{gen} \tag{4}$$

where $\Sigma_{gen} = \overline{|\nabla c|}$ is the generalised FSD (Boger et al. 1998; Poinsot and Veynante 2001), $S_d = (Dc/Dt)/|\nabla c|$ is the displacement speed and $\overline{(q)}_s = \overline{q|\nabla c|}/\overline{|\nabla c|}$ is the surface averaged value of a general variable q (Trouvé and Poinsot 1994; Boger et al. 1998). The transport equation of Σ_{gen} is given by (Pope 1988; Candel and Poinsot 1990):

$$\partial \Sigma_{gen}/\partial t + \partial (\tilde{u}_j \Sigma_{gen})/\partial x_j = \underbrace{-\partial \left\{ \left[\overline{(u_k)}_s - \tilde{u}_k \right] \Sigma_{gen} \right\}/\partial x_k}_{T_1-turbulent\ transport}$$

$$+ \underbrace{\overline{\left((\delta_{ij} - N_i N_j) \partial u_i/\partial x_j \right)}_s \Sigma_{gen}}_{T_2-strain\ rate} \underbrace{-\partial \left[\overline{(S_d N_k)}_s \Sigma_{gen} \right]/\partial x_k}_{T_3-propagation} + \underbrace{\overline{(S_d \partial N_i/\partial x_i)}_s \Sigma_{gen}}_{T_4-curvature} \tag{5}$$

where $\vec{N} = -\nabla c/|\nabla c|$ is the local flame normal vector. In Eq. (5), T_1 is the turbulent transport term. The term T_2 is commonly referred to as the strain rate term because it originates due to the tangential strain rate $a_T = (\delta_{ij} - N_i N_j)\partial u_i/\partial x_j$, whereas T_3 is referred to as the FSD propagation term and T_4 is known as the FSD curvature term because it arises as a result of flame curvature $\kappa_m = 0.5\nabla \cdot \vec{N} = 0.5(\partial N_i/\partial x_i)$. All the terms on the right-hand side of Eq. (5) (i.e., T_1, T_2, T_3 and T_4) are unclosed and therefore they need to be modelled. The modelling of T_1, T_2, T_3 and T_4 will be discussed in detail in Sect. 4 of this paper.

3 Numerical Implementation

DNS simulations of statistically planar premixed flames for different turbulence intensities for two different integral length scale to flame thickness ratios have been considered for this analysis. These simulations have been conducted using a well-known compressible DNS code SENGA+ (Jenkins and Cant 1999). In SENGA+, the conservation equations of mass, momentum, energy, and species are solved in non-dimensional form. In SENGA+, all first and second-order derivatives for the internal grid points are evaluated using a 10th order central difference scheme but the order of accuracy gradually drops to a one-sided 2nd order scheme at the non-periodic boundaries (Jenkins and Cant 1999). An explicit 3rd order Runge–Kutta scheme (Wray 1990) is used for the time-advancement of all governing equations. All the simulations consider inlet and outlet boundaries in the direction of mean flame propagation, whereas transverse boundaries are considered to be periodic. The outflow boundary is considered to be partially non-reflecting and specified according to the well-known Navier–Stokes Characteristic Boundary Conditions (NSCBC) technique (Poinsot and Lele 1992). Here the mean inlet velocity U_{mean} was gradually altered to match the turbulent burning velocity in order to ensure that the flame remains stationary in the statistical sense within the computational domain. A well-known pseudo-spectral method (Rogallo 1981) is used to initialise the fluctuating velocity field by a homogeneous isotropic incompressible distribution following the Batchelor-Townsend spectrum (Batchelor and Townsend 1948) for prescribed

values of root-mean-square turbulent velocity u' and the integral length scale of turbulence l. The reacting scalar field is initialised by a unstretched laminar flame solution. A modified bandwidth filtered forcing method (Klein et al. 2017) in physical space is used for the current analysis, which yields a forcing term proportional to $(1 - c)$ in the momentum equation such that the forcing is employed for the unburned gas ahead of the flame. This forcing scheme maintains both the required values of root-mean-square velocity u' and the integral length scale of turbulence le_d in the unburned gas (i.e., $c < 0.001$). Table 1 lists the simulation domain size, the uniform Cartesian grid for discretisation along with the inlet values of root-mean-square turbulent velocity fluctuation normalised by the unstrained laminar burning velocity u'/S_L, integral length scale to the Zel'dovich flame thickness ratio l/δ_z, Damköhler number $Da = lS_L/u'\delta_z$, Karlovitz number $Ka = \left(u'/S_L\right)^{3/2}\left(l/\delta_z\right)^{-1/2}$ and heat release parameter $\tau = (T_{ad} - T_0)/T_0$ where the Zel'dovich flame thickness δ_z is defined as: $\delta_z = \alpha_{T0}/S_L$ with α_{T0} and S_L being the thermal diffusivity and unstrained laminar burning velocity, respectively. The locations of these cases on Borghi-Peters diagram (Peters 2000) are shown in Fig. 1, which shows that the cases considered here span from the wrinkled flamelet regime to the high Karlovitz number thin reaction zones regime. The grid spacing used here ensures at least 10 grid points within $\delta_{th} = (T_{ad} - T_0)/\max|\nabla T|_L$ with T, T_0 and T_{ad} being the dimensional temperature, unburned gas temperature and the adiabatic flame temperature, respectively. This implies that the steepest gradients of temperature and reaction progress variable have been resolved using at least 10 grid points. Moreover, the reaction zone for the present thermochemistry (i.e., $0.4 < c < 0.95$) has at least 10 grid points for the current database. Moreover, at least 1.5 grid points are kept within the Kolmogorov length scale η for the simulation parameters considered here. The values of $l/\delta_z = 2.625$ and 5.25 correspond to $l/\delta_{th} = 1.5$ and 3.0 for the present thermochemistry. The chemical mechanism is simplified by a single-step Arrhenius mechanism representing stoichiometric methane-air flame in this analysis in the interests of the computational economy for a detailed parametric analysis. The Lewis number of all the species is taken to be unity and the gaseous mixture is taken to obey the ideal gas law. Standard values are considered for Prandtl number (i.e., $Pr = 0.7$), Zel'dovich number (i.e., $\beta = T_{ac}\left(T_{ad} - T_0\right)/T_{ad}^2 = 6.0$ with T_{ac} being the activation temperature) and the ratio of specific heats (i.e., $\gamma = 1.4$). It was demonstrated that the flame propagation and reactive scalar statistics obtained from

Table 1 Simulation parameters for all cases considered

	u'/S_L	l/δ_z	Da	Ka	τ	Domainsize	Grid size
Case—A1	1.0	5.25	5.25	0.44	4.5	$140.7\,\delta_z \times (70.35\,\delta_z)^2$	$800 \times (400)^2$
Case—A2	1.0	2.625	2.625	0.62	4.5	$105.5\,\delta_z \times (35.18\,\delta_z)^2$	$600 \times (200)^2$
Case—B1	3.0	5.25	1.75	2.27	4.5	$140.7\,\delta_z \times (70.35\,\delta_z)^2$	$800 \times (400)^2$
Case—B2	3.0	2.625	0.875	3.21	4.5	$105.5\,\delta_z \times (35.18\,\delta_z)^2$	$600 \times (200)^2$
Case—C1	5.0	5.25	1.05	4.88	4.5	$140.7\,\delta_z \times (70.35\,\delta_z)^2$	$800 \times (400)^2$
Case—C2	5.0	2.625	0.525	6.90	4.5	$105.5\,\delta_z \times (35.18\,\delta_z)^2$	$600 \times (200)^2$
Case—D1	7.5	5.25	0.7	8.96	4.5	$140.7\,\delta_z \times (70.35\,\delta_z)^2$	$800 \times (400)^2$
Case—D2	7.5	2.625	0.35	12.68	4.5	$105.5\,\delta_z \times (35.18\,\delta_z)^2$	$600 \times (200)^2$
Case—E1	10.0	5.25	0.525	13.80	4.5	$140.7\,\delta_z \times (70.35\,\delta_z)^2$	$800 \times (400)^2$
Case—E2	10.0	2.625	0.2625	19.52	4.5	$105.5\,\delta_z \times (35.18\,\delta_z)^2$	$600 \times (200)^2$

Fig. 1 The cases considered here on the Borghi–Peters regime diagram
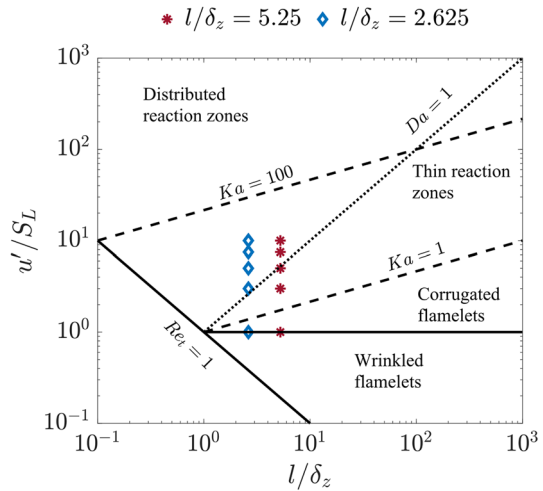
simple chemistry DNS of stoichiometric methane-air premixed flames remain in good qualitative agreement with the corresponding detailed chemistry simulations (Keil et al. 2021a, b). The quantitative differences remain comparable to the uncertainties associated with the different definitions of reaction progress variable in detailed chemistry simulations (Keil et al. 2021b).

All the simulations listed in Table 1 have been conducted until the desired values of turbulent kinetic energy and integral length scale have been obtained and also the turbulent burning velocity S_T and flame surface area A_T reach statistically stationary states. The readers are directed to Varma et al. (2021) to find out statistically steady nature of volume integrated FSD transport for the database considered in this work. This simulation time remains greater than the through-pass time (i.e., $t_{sim} > L_x/U_{mean}$) and at least 10 eddy turn over times (i.e., $t_{sim} > 10l/u'$) for all cases.

In order to obtain Reynolds/Favre averaged quantities, the quantities of interest are averaged in the transverse directions normal to the mean flame propagation (i.e., homogeneous directions) and also in time over 2 chemical times (i.e., $2t_c = 2\delta_z/S_L$) following previous analyses (Trouvé and Poinsot 1994; Veynante et al. 1997; Katragadda et al. 2011, 2014a; Chakraborty and Cant 2011, 2013; Sellmann et al. 2017; Varma et al. 2022a). For statistically planar flames, the Favre-averaged reaction progress variable $\widetilde{c}$ is a function of the coordinate in the direction of mean flame propagation (i.e., x-direction). As all the terms in the FSD transport equation and $\widetilde{c}$ are functions of x, the results presented in this paper are not dependent on the averaging over bins of $\widetilde{c}$. Thus, all the quantities in Sect. 4 will be presented as a function of $\widetilde{c}$ for the sake of generality. These results do not change appreciably (i.e., the maximum variation is of the order of 2%) if the distinct half of the domain and half of the time duration of averaging are considered instead of the full sample size and time series, as used in the results section of this paper.

4 Results and Discussion

4.1 Flame-Turbulence Interaction and Statistical Behaviour of the FSD

The reaction progress variable c isosurfaces when the flames have reached statistically stationary state are shown in Fig. 2. It can be seen from Fig. 2 that the extent of flame wrinkling increases with increasing u'/S_L for a given value of l/δ_z, as expected. Figure 2 further shows that the extent of flame wrinkling also increases with increasing l/δ_z for a given value of u'/S_L. The observations from Fig. 2 can be substantiated from the variations of the values of normalised flame surface area A_T/A_L and normalised turbulent burning velocity S_T/S_L, which are shown Fig. 3. Here, A_T and S_T are defined as $A_T = \int_V |\nabla c| dV$ and $S_T = (\rho_0 A_L)^{-1} \int_V \dot{\omega} dV$ where A_L is the projected flame surface area in the direction of mean flame propagation. Figure 3 shows that A_T/A_L increases with increasing l/δ_z for a given value of u'/S_L, which is also reflected with an increase in S_T/S_L with an increase in

Fig. 2 Instantaneous views of reaction progress variable $c = 0.1, 0.5$ and 0.9 isosurfaces for cases with $l/\delta_z = 2.625$ (left column) and 5.25 (right column). Note different dimensions of the domain between $l/\delta_z = 2.625$ and 5.25 cases
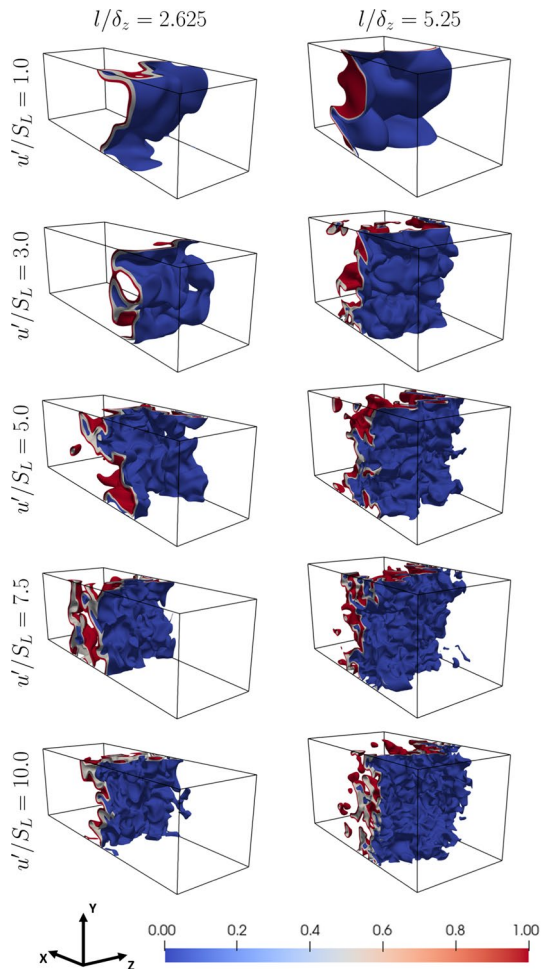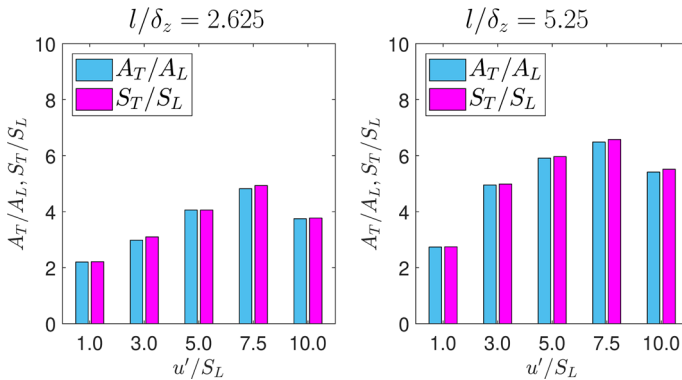
Fig. 3 Variations of A_T/A_L and S_T/S_L with u'/S_L for all cases considered here

l/δ_z for a given value of u'/S_L. Moreover, for a given value of l/δ_z, the normalised flame surface area A_T/A_L increases monotonically with increasing u'/S_L before the bending occurs, which is observed for $u'/S_L \geq 7.5$ for the DNS database considered here (Ahmed et al. 2019; Varma et al. 2021). The normalised flame surface area A_T/A_L can be parameterised as: $A_T/A_L = \left(\eta_o/\eta_c\right)^{D_f-2}$ where η_c and η_o are respectively the inner and outer cut-off length scales and D_f (with $D_f > 2$) (Gouldin et al. 1989; Chakraborty and Klein 2008; Tamadonfar and Gülder 2014; Ahmed et al. 2019) is the fractal dimension of the flame surface. The inner cut-off scale η_c can be taken to scale with the flame thickness δ_z (Knikker et al. 2002; Chakraborty and Klein 2008) and the integral length scale l is usually taken to be the measure of the outer cut-off scale η_o in the context of RANS (Gouldin et al. 1989; Poinsot and Veynante 2001). This suggests that A_T/A_L scales with $\left(l/\delta_z\right)^{D_f-2}$, which implies that A_T/A_L is expected to increase with increasing l/δ_z. Further physical explanations behind an increase in A_T/A_L with increasing l/δ_z for a given value of u'/S_L and the bending behaviour have been discussed elsewhere (Ahmed et al. 2019; Varma et al. 2021) in detail for this database and thus are not repeated here. For these statistically planar flame cases, Damköhler's first hypothesis (i.e., $S_T/S_L = A_T/A_L$) is maintained (Ahmed et al. 2019; Varma et al. 2021) and the physical explanations for the validity of Damköhler's first hypothesis for statistically planar flames were provided elsewhere (Chakraborty et al. 2019) and thus are not repeated here.

The variations of $\Sigma_{gen} \times \delta_z$ with $\tilde{c}$ for all cases considered here are shown in Fig. 4 (first column). It can be seen from Fig. 4 (first column) that the peak value of Σ_{gen} mostly increases (mildly) with increasing u'/S_L, whereas the peak value of Σ_{gen} for smaller values of l/δ_z is significantly greater than the higher value of l/δ_z. In order to understand this behaviour of $\Sigma_{gen} = \Xi \times |\nabla \bar{c}|$, it is worthwhile to consider the variations of $|\nabla \bar{c}|$ and Ξ with $\tilde{c}$, which are also shown in Fig. 4 (second and third columns, respectively). Here, wrinkling factor Ξ is defined as: $\Xi = \Sigma_{gen}/|\nabla \bar{c}|$ (Weller et al. 1998; Charlette et al. 2002). It can be seen from Fig. 4 (second column) that the peak value of $|\nabla \bar{c}|$ is smaller for higher values of l/δ_z. The turbulent flame brush thickness can be quantified as $\delta_b \sim 1/max|\nabla \bar{c}|$, and thus a smaller peak value of $|\nabla \bar{c}|$ for higher values of l/δ_z is representative of a thicker flame brush because of greater extent of flame wrinkling (see Fig. 2). The greater extent of flame wrinkling for higher values of l/δ_z is reflected in the higher values of wrinkling factor Ξ, as shown in Fig. 4 (third column). However, the decrease in $|\nabla \bar{c}|$ with an increase in l/δ_z
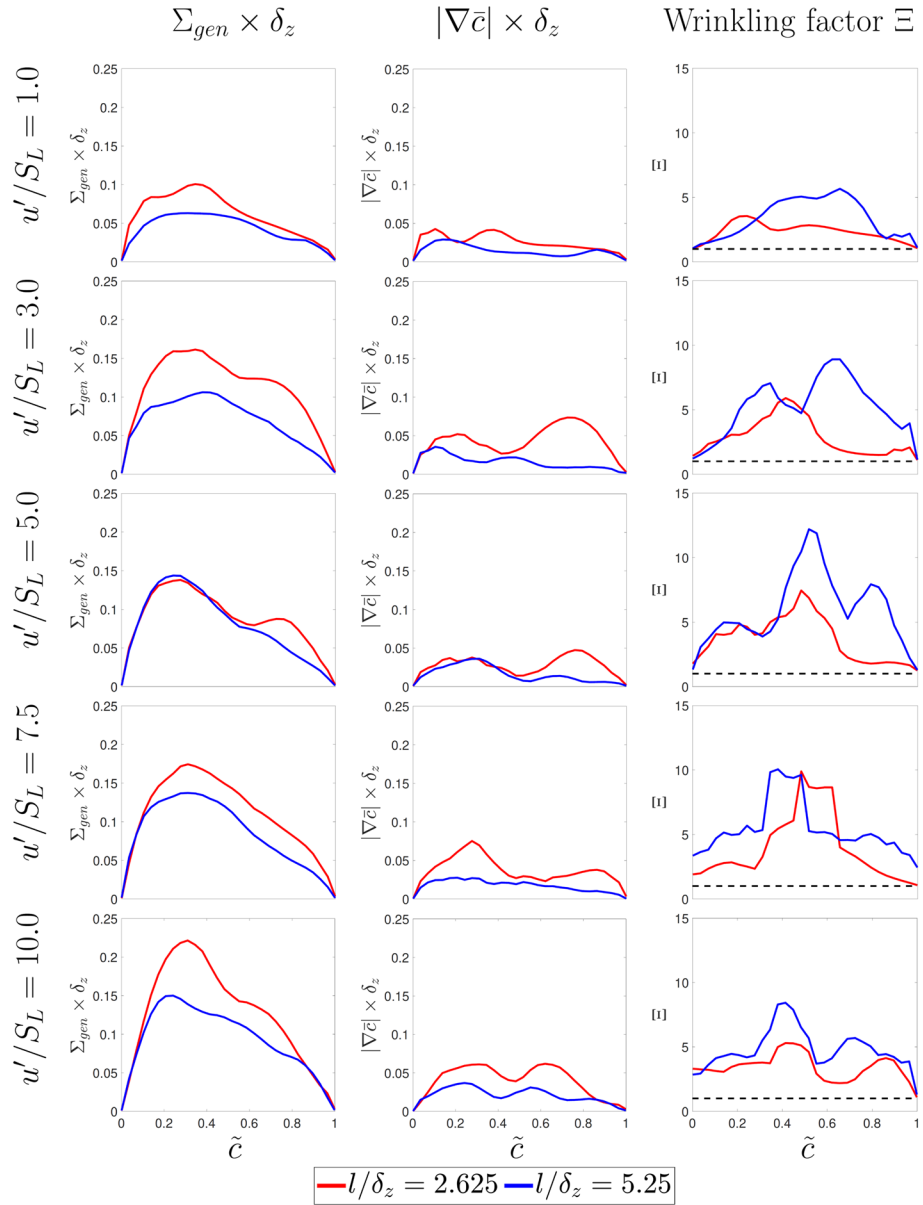
Fig. 4 Variations of generalised FSD $\Sigma_{gen} \times \delta_z$ (first column), resolved FSD $|\nabla\bar{c}| \times \delta_z$ (second column) and wrinkling factor Ξ (third column) with $\tilde{c}$ for all cases considered. The black dashed line represents the minimum possible value of wrinkling factor (i.e., $\Xi = 1.0$)

overwhelms the increase in Ξ to give rise to a decrease in peak values of $\Sigma_{gen} = \Xi \times |\nabla\bar{c}|$ with an increase in l/δ_z.

4.2 Variations of the Unclosed Terms in the FSD Transport Equation

The challenges of algebraic closures of Σ_{gen} in the context of RANS were discussed elsewhere (Ahmed et al. 2021; Rasool et al. 2022) and qualitatively similar results have been obtained for the present database so will not be discussed further. Instead, the present analysis will focus on the effects of u'/S_L and l/δ_z on the unclosed terms of the FSD Σ_{gen} transport equation. The variations of the normalised unclosed terms of the FSD transport equation (i.e., $\{T_1, T_2, T_3, T_4\} \times \delta_z^2/S_L$) with $\widetilde{c}$ are shown in Fig. 5 for the cases considered here. It can be seen from Fig. 5 that the qualitative behaviours of the terms of the FSD transport equation are not influenced by l/δ_z but the magnitudes of the leading order source and sink contributions by the strain rate term T_2 and the curvature term T_4, respectively are smaller for higher values of l/δ_z. Moreover, the magnitudes of the leading order source and sink contributions of T_2 and T_4, respectively increase with increasing u'/S_L for a given value of l/δ_z. It can be seen from Fig. 5 that the strain rate term T_2 acts as a leading order source for all cases, where T_4 assumes positive values towards the unburned gas side of the flame brush and becomes negative towards the burned gas side for small turbulence intensities (e.g., $u'/S_L = 1.0$ and 3.0) but for high turbulence intensities (e.g., $u'/S_L = 7.5$ and 10.0) the curvature term T_4 predominantly assumes negative values throughout the flame brush. The propagation term T_3 and the turbulent transport term T_1 assume locally positive and negative values within the flame brush but the magnitude of their relative contributions in comparison to the magnitudes of T_2 and T_4 diminish with increasing u'/S_L. These behaviours are qualitatively similar to previous studies for both simple (Trouvé and Poinsot 1994; Chakraborty and Cant 2011, 2013; Varma et al. 2022a) and detailed (Luca et al. 2019; Papaposolou et al. 2019; Berger et al. 2022) chemistry and also with the scaling arguments by Chakraborty and Cant (2013). The modelling of these unclosed terms will be addressed next in this paper.

4.3 Modelling of the Turbulent Transport Term T_1

Equation 5 indicates that the closure of the turbulent transport term T_1 depends on the modelling of the turbulent flux of the generalised FSD $\left[\overline{(u_i)}_s - \widetilde{u}_i\right]\Sigma_{gen}$. The conventional way to close $\left[\overline{(u_i)}_s - \widetilde{u}_i\right]\Sigma_{gen}$ is to employ a classical gradient hypothesis (Poinsot and Veynante 2001; Hawkes and Cant 2000, 2001):

$$\left[\overline{(u_i)}_s - \widetilde{u}_i\right]\Sigma_{gen} = -(v_t/Sc_\Sigma)\partial\Sigma_{gen}/\partial x_i \tag{6}$$

Here $v_t = C_\mu \widetilde{k}^2/\widetilde{\epsilon}$ is the kinematic eddy viscosity, $C_\mu = 0.09$ is the model parameter and Sc_Σ is a suitable turbulent Schmidt number with $\widetilde{k} = \overline{\rho u_i'' u_i''}/2\overline{\rho}$ and $\widetilde{\epsilon} = \overline{\mu(\partial u_i''/\partial x_j)(\partial u_i''/\partial x_j)}/\overline{\rho}$ being the turbulent kinetic energy and its dissipation rate, respectively (Poinsot and Veynante 2001; Hawkes and Cant 2000, 2001). The only non-zero component of the FSD flux is $\left[\overline{(u_1)}_s - \widetilde{u}_1\right]\Sigma_{gen}$ for statistically planar flames propagating in the negative x_1- direction. The variations of $\left[\overline{(u_1)}_s - \widetilde{u}_1\right]\Sigma_{gen} \times \delta_z/S_L$ and $(\partial\Sigma_{gen}/\partial x_1) \times \delta_z^2$ with $\widetilde{c}$ for all cases considered here are shown in Figs. 6 and 7, respectively. A comparison between Figs. 6 and 7 reveals that $\left[\overline{(u_1)}_s - \widetilde{u}_1\right]\Sigma_{gen}$ and $(\partial\Sigma_{gen}/\partial x_1)$
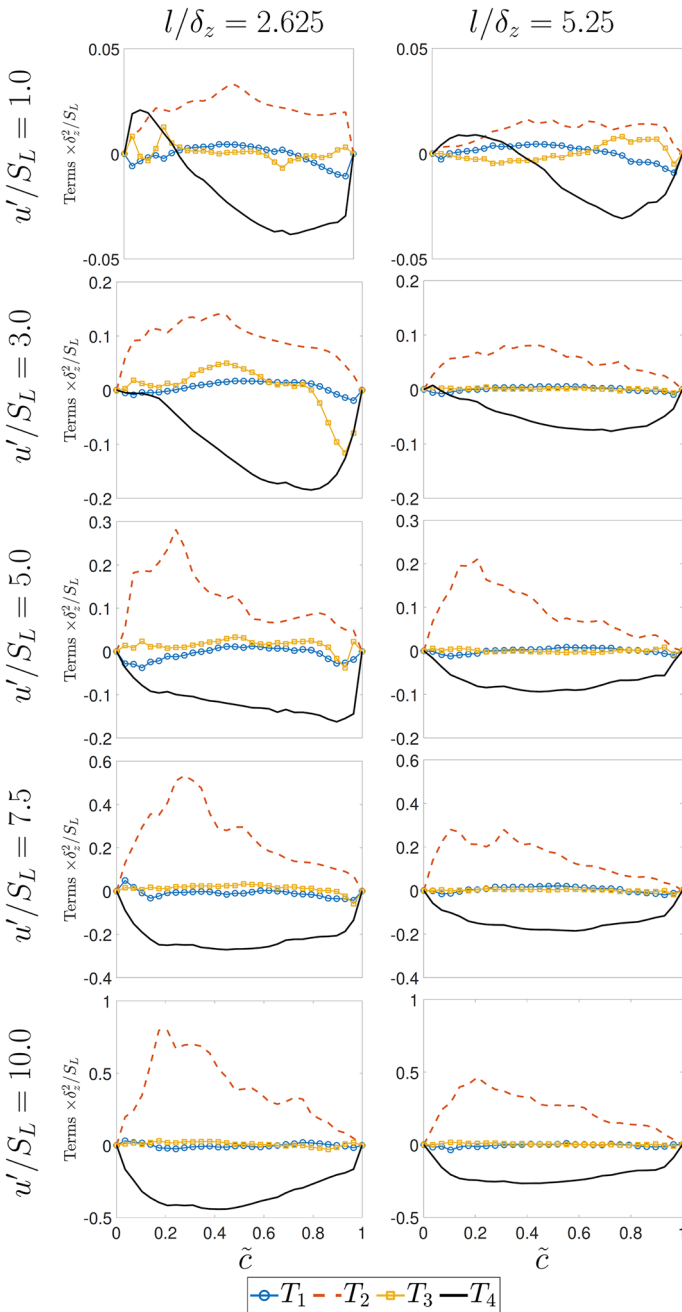
Fig. 5 Variations of the normalised unclosed terms of the FSD transport equation $\{T_1, T_2, T_3, T_4\} \times \delta_z^2/S_L$ with $\tilde{c}$ for $l/\delta_z = 2.625$ (left) and 5.25 (right) and for $u'/S_L = 1.0, 3.0, 5.0, 7.5$ and 10.0 (1st–5th row)

show different signs for a major part of the flame brush and this tendency is particularly prevalent for small values of turbulence intensity. This suggests $\left[\overline{(u_1)}_s - \tilde{u}_1\right]\Sigma_{gen}$ exhib-

its counter-gradient transport for small values of u'/S_L and therefore the gradient hypothesis based model given by Eq. (6) is not suitable for the purpose of modelling $\left[\overline{(u_1)}_s - \tilde{u}_1\right]\Sigma_{gen}$ and therefore its prediction is not shown in Fig. 6.

Previously a model for the turbulent flux of generalised FSD was proposed by Chakraborty and Cant (2009b, 2011) in the following manner, which can predict both gradient and counter-gradient behaviour:

$$\left[\overline{(u_1)}_s - \tilde{u}_i\right]\Sigma_{gen} = \frac{\left(1 - 2\tilde{c}\right)\overline{\rho u_i'' c''}\Sigma_{gen}}{\overline{\rho c''^2} + \overline{\rho c}\left(1 - \tilde{c}\right)} \tag{7}$$

This model accounts for the fact the FSD flux $\left[\overline{(u_1)}_s - \tilde{u}_i\right]\Sigma_{gen}$ exhibits a counter-gradient (gradient) behaviour when $\overline{\rho u_i'' c''}$ shows a counter-gradient (gradient) transport. It can be seen from Fig. 6 that the model given by Eq. (7) provides satisfactory prediction of $\left[\overline{(u_1)}_s - \tilde{u}_i\right]\Sigma_{gen}$ for all cases considered here. The competition between turbulent velocity fluctuation $\sqrt{2\tilde{k}/3}$ and the velocity jump due to heat release τS_L determines the nature of turbulent transport (Veynante et al. 1997; Chakraborty and Cant 2009b-d) and thus l/δ_z is unlikely have any influence on the closure of $\left[\overline{(u_1)}_s - \tilde{u}_i\right]\Sigma_{gen}$. Although Eq. (7) captures the qualitative behaviour of $\left[\overline{(u_1)}_s - \tilde{u}_i\right]\Sigma_{gen}$, there is a scope for improvement for quantitative agreement. As the magnitude of T_1 remains small in comparison to the leading order contributions of T_2 and T_4 and thus the modelling inaccuracies of T_1 using Eq. (7) is not expected to affect the closure of the Σ_{gen} transport equation. Moreover, it is worth noting that the successful performance of Eq. (7) depends on the successful closures of $\overline{\rho u_1'' c''}$ and $\overline{\rho c''^2}$, which have been addressed elsewhere (Veynante et al. 1997; Chakraborty and Cant 2009b-d; Chakraborty and Swaminathan 2011; Varma et al. 2022b) and will not be addressed further in this paper.

## 4.4 Modelling of the Turbulent Strain Rate Term T_2

The tangential strain rate term T_2 is traditionally modelled by splitting it in the following manner (Cant et al. 1990; Candel et al. 1990; Poinsot and Veynante 2001):

$$T_2 = \underbrace{\left[\delta_{ij} - \overline{(N_i N_j)}_s\right]\frac{\partial \tilde{u}_i}{\partial x_j}\Sigma_{gen}}_{S_R} + \underbrace{\overline{\left(\left(\delta_{ij} - N_i N_j\right)\frac{\partial u_i''}{\partial x_j}\right)_s}\Sigma_{gen}}_{S_{UR}} \tag{8}$$

where S_R and S_{UR} are the resolved and unresolved components of the strain rate term, respectively. It can be appreciated from Eq. (8) that the closure of S_R depends on the closures of the orientation factors $\overline{(N_i N_j)}_s$, which is modelled by Cant et al (1990) as: $\overline{(N_i N_j)}_s = \overline{(N_i)}_s\overline{(N_j)}_s + (\delta_{ij}/3)\left[1 - \overline{(N_k)}_s\overline{(N_k)}_s\right]$ where $\overline{(N_i)}_s = -(\partial \bar{c}/\partial x_i)/\Sigma_{gen}$ is the ith component of the surface averaged flame normal vector. However, $\tilde{c}$ is obtained from RANS simulations but $\bar{c}$ needs to be extracted from $\tilde{c}$ in order to evaluate $\overline{(N_i)}_s$. A presumed bimodal probability density function of c with impulses at $c = 0$ and $c = 1.0$ yields
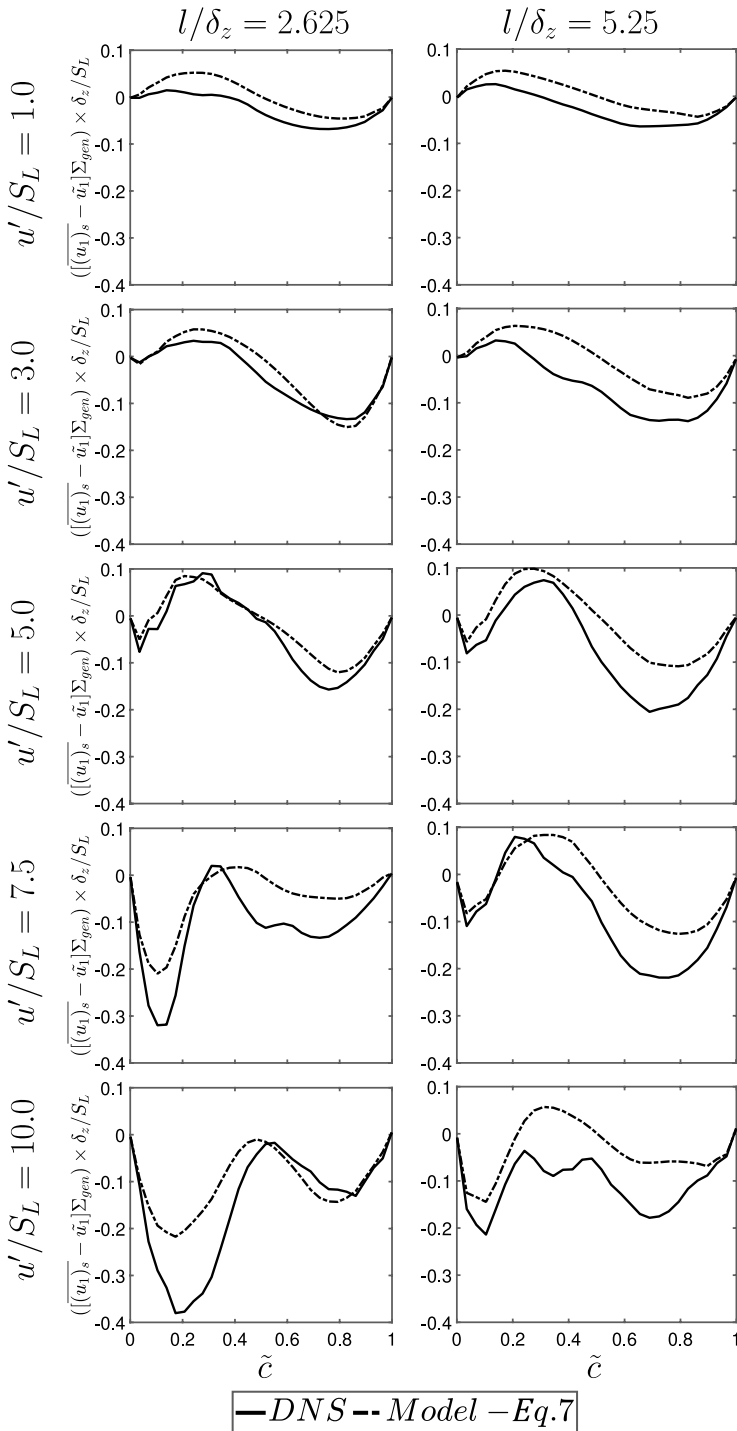
Fig. 6 Variation of $\left[\overline{(u_i)}_s - \widetilde{u}_i\right]\Sigma_{gen} \times \delta_z/S_L$ with $\widetilde{c}$ for $l/\delta_z = 2.625$ (left) and 5.25 (right) along with the predictions of Eq. (7) for $u'/S_L = 1.0, 3.0, 5.0, 7.5$ and 10.0 (1st–5th row)
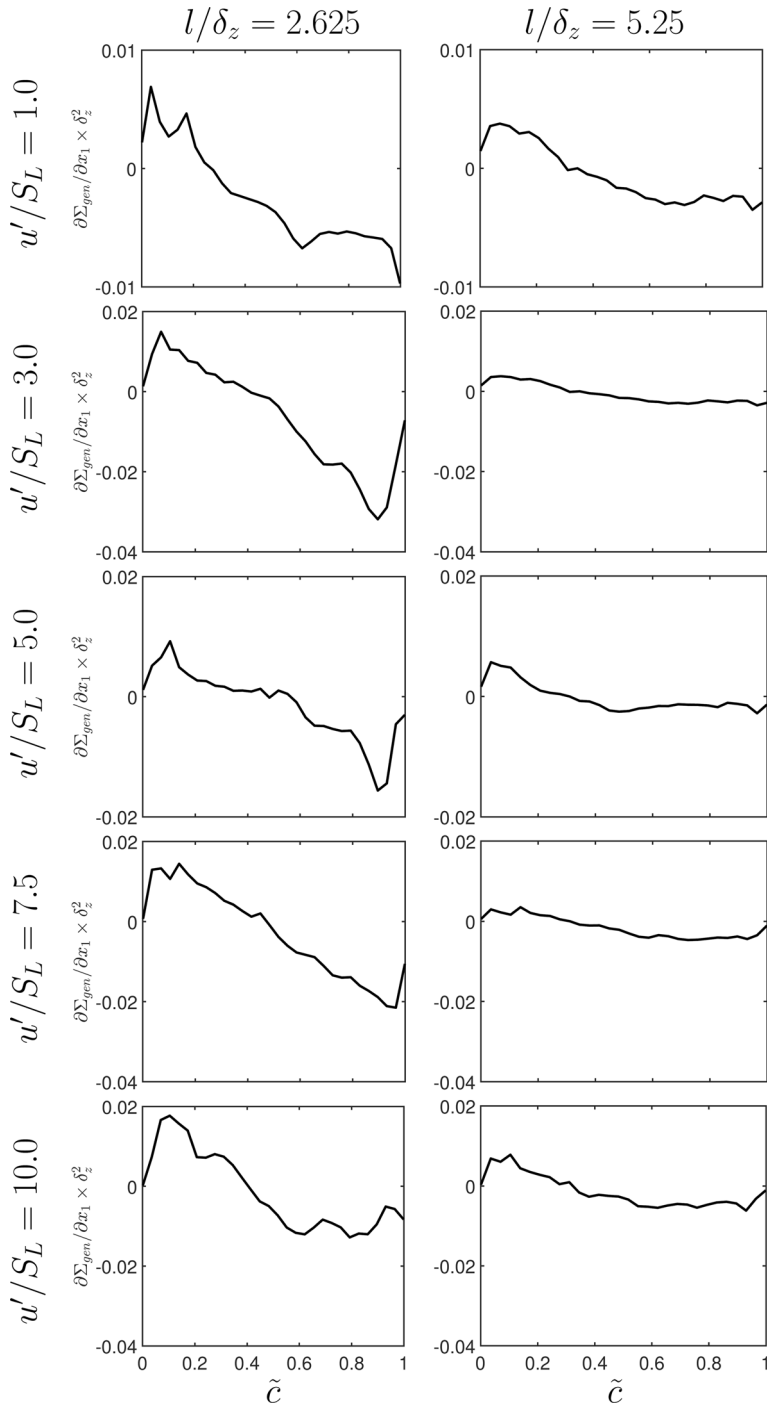
Fig. 7 Variation of $(\partial \Sigma_{gen}/\partial x_1) \times \delta_z^2$ with $\widetilde{c}$ along for $l/\delta_z = 2.625$ (left) and 5.25 (right) and for $u'/S_L = 1.0, 3.0, 5.0, 7.5$ and 10.0 (1st–5th row)

$\bar{c} = (1 + \tau)\tilde{c}/(1 + \tau\tilde{c}) + O(\gamma)$, where $O(\gamma)$ accounts for the contribution of the burning mixture (Bray et al. 1985), which is expected to be negligible for large values of Damköhler number (i.e., $Da \gg 1$). However, PDFs of c cannot be approximated by a bi-modal distribution in the thin reaction zones regime flames with $Da < 1$. Therefore, Katragadda et al. (2011) proposed a modification to the BML expression for $\bar{c}$ for $Da < 1$ in the following manner: $\bar{c} = (1 + \tau.g^a)\tilde{c}/(1 + \tau.g^a\tilde{c})$ where $g = \overline{c''^2}/[\tilde{c}(1 - \tilde{c})]$ is the segregation factor, and $a = 1.5$ is a model parameter. An alternative expression for $\bar{c}$ was proposed by Bray et al. (2011) in the following manner: $\bar{c} = \tilde{c} + \tau\overline{\rho c''^2}/\rho_0$. It was demonstrated elsewhere (Ahmed et al. 2021; Rasool et al. 2022) that $\bar{c}$ models proposed by Katragadda et al. (2011) and Bray et al. (2011) exhibit comparable performance and satisfactorily predicts $\bar{c}$ extracted from DNS data. The same conclusion holds also for this study and thus the predictions of $\bar{c} = (1 + \tau.g^a)\tilde{c}/(1 + \tau.g^a\tilde{c})$ and $\bar{c} = \tilde{c} + \tau\overline{\rho c''^2}/\rho_0$ are not explicitly shown here for the sake of conciseness.

Another alternative model for $\overline{(N_i N_j)}_s$ was proposed by Veynante et al. (1996), which is given as: $\overline{(N_i N_{j=i})}_s = \sum_{k \neq i} \widetilde{u''_k u''_k}/4\tilde{k}$ and $\overline{(N_i N_{j \neq i})}_s = \widetilde{u''_i u''_j}/2\tilde{k}$. The models by Veynante et al. (1996) and Cant et al. (1990) will henceforth be referred to as the VPDM and MCPB models, respectively. The predictions of these models are compared to the variation of S_R with $\tilde{c}$ across the flame brush, as obtained from DNS data, in Fig. 8. Figure 8 shows that the predictions of the MCPB model mostly captures S_R behaviour obtained from DNS data, although it slightly underpredicts the magnitude of S_R especially for small values of u'/S_L (e.g., $u'/S_L = 1.0$ and 3.0). The VPDM model, on the other hand, overpredicts S_R values for $u'/S_L = 3.0$ and 5.0 towards the burned gas side for $l/\delta_z = 2.625$ but a satisfactory agreement between DNS data and VPDM model is obtained for $l/\delta_z = 5.25$.

The discrepancy between model predictions and DNS data in the modelling of S_R originates due to the uncertainty of closure of the orientation factors $\overline{(N_i N_j)}_s$. Cant et al. (1990) assume isotropic distribution of the fluctuating part of the flame normal components while deriving the MCPB model. However, experimental analysis by Veynante et al. (1996) and DNS data by Chakraborty and Cant (2006) revealed that the assumption of the isotropic fluctuation of the flame normal vector does not remain valid especially for small and moderate turbulence intensities. This is responsible for the underprediction of S_R by the MCPB model. Although the VPDM model does not assume isotropic nature of fluctuating part of the flame normal components, but the modelling inaccuracies involved in estimating $\overline{(N_i N_j)}_s$ leads to the disagreement between the VPDM model and DNS data in Fig. 8. The level of isotropy of flame normal component fluctuations is expected to hold better for smaller values of l/δ_z (e.g., $l/\delta_z = 2.625$) and thus the VPDM model performs relatively better for higher values of l/δ_z (e.g., $l/\delta_z = 5.25$) where the aforementioned isotropy effects are expected to be weak.

The unresolved component S_{UR} is modelled by the models proposed by Cant et al. (1990) and Candel et al. (1990), which will henceforth be referred to as the SCPB and SCFM models, respectively. According to Cant et al. (1990) S_{UR} is modelled as $S_{UR} = 0.28\sqrt{\tilde{\epsilon}/\nu_0}\Sigma_{gen}$, where ν_0 is the kinematic viscosity of the unburned gas. By contrast, the SCFM model considers $S_{UR} = a_0\Gamma_k\left(\tilde{\epsilon}/\tilde{k}\right)\Sigma_{gen}$, where $a_0 = 2.0$ is a model parameter and Γ_k is the efficiency function (as proposed by Meneveau and Poinsot (1991)) which is a function of l_t/δ_z and $\sqrt{2\tilde{k}/3}/S_L$ and $l_t = C_k\tilde{k}^{3/2}/\tilde{\epsilon}$ is the local integral length scale where $C_k = 1.5$ (Sreenivasan 1984). The predictions of the SCPB and SCFM models are shown along with the S_{UR} extracted from the DNS data in Fig. 9. It can be seen from Fig. 9 that both SCPB and SCFM models significantly overpredict S_{UR} for all cases. The extent of
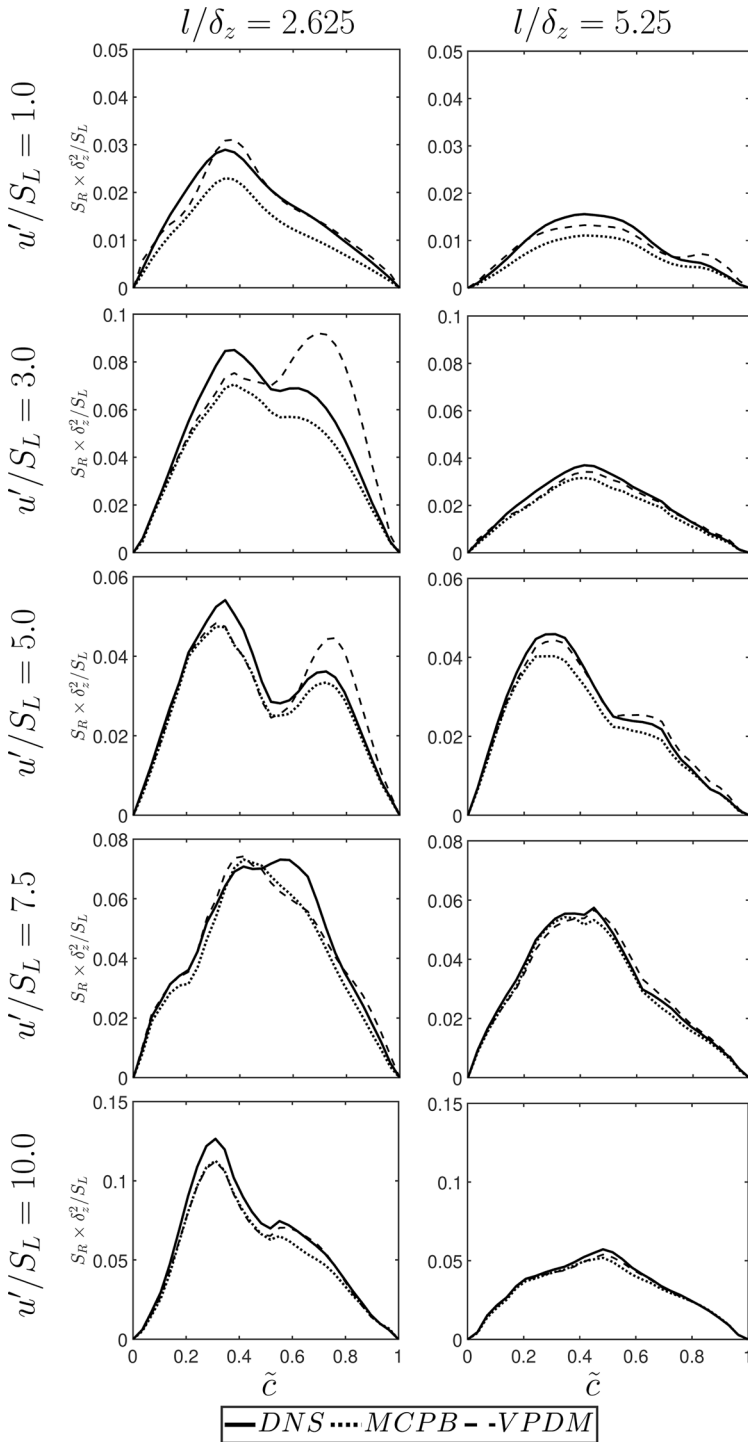
Fig. 8 Variation of $S_R \times \delta_z^2/S_L$ with $\widetilde{c}$ for $l/\delta_z = 2.625$ (left) and 5.25 (right) along with the predictions of the MCPB and VPDM models for $u'/S_L = 1.0, 3.0, 5.0, 7.5$ and 10.0 (1st–5th row)
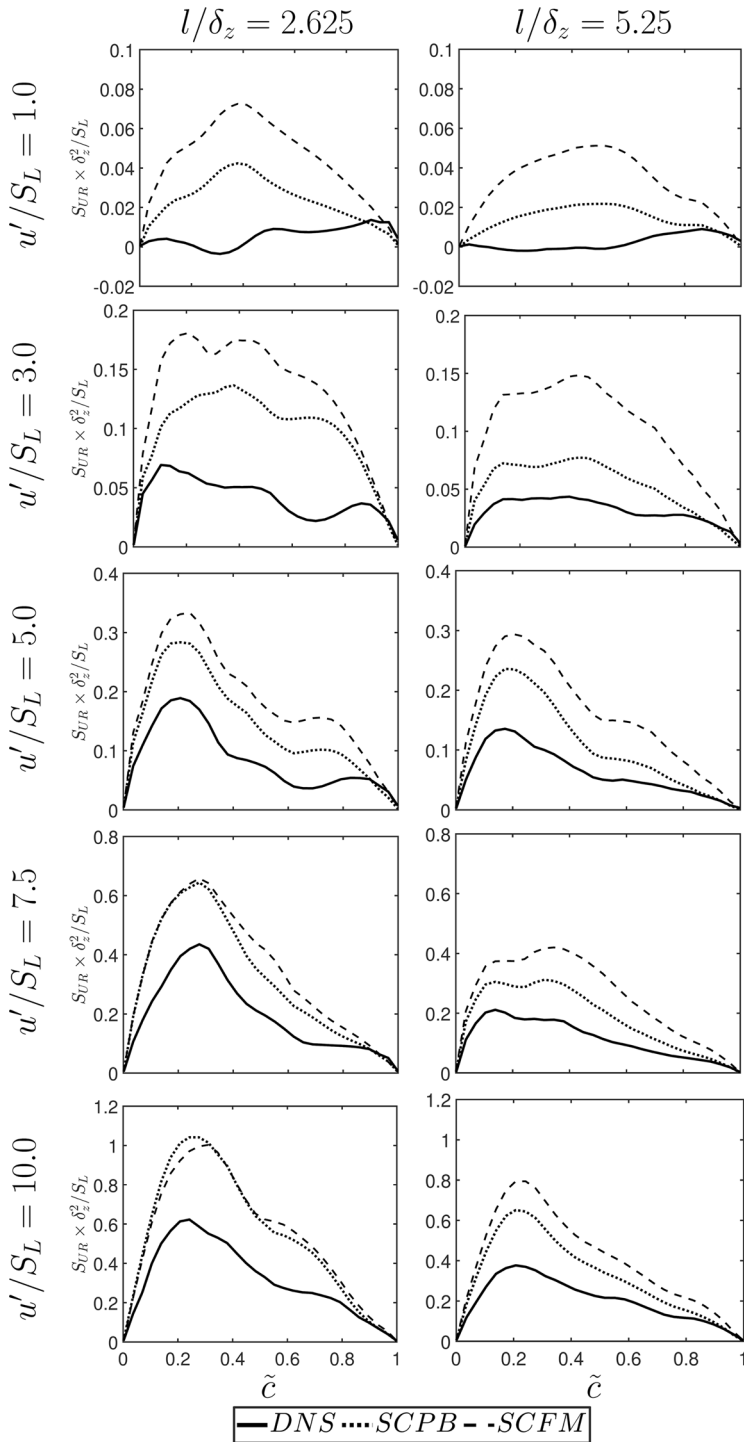
Fig. 9 Variation of $S_{UR} \times \delta_z^2/S_L$ with $\tilde{c}$ for $l/\delta_z = 2.625$ (left) and 5.25 (right) along with the predictions of the SCPB and SCFM models for $u'/S_L = 1.0$, 3.0, 5.0, 7.5 and 10.0 (1st–5th row)

this overprediction is greater for the SCFM model than the SCPB model for small values of turbulence intensity (e.g., $u'/S_L = 1.0$ and 3.0) but the predictions of these models become comparable for large values of turbulence intensity (e.g., $u'/S_L = 10.0$). Moreover, S_{UR} assumes locally small negative values for $u'/S_L = 1.0$ for both $l/\delta_z = 2.625$ and 5.25 whereas both SCPB and SCFM models can only predict positive values.

It is worth noting that both SCPB and SCFM models consider only the turbulent time scale to model S_{UR}. The SCPB model considers the Kolmogorov timescale (i.e., $\sqrt{\nu_0/\epsilon}$), whereas the SCFM model accounts for large scale turbulent timescale (i.e., $\widetilde{k}/\widetilde{\epsilon}$) but the unsatisfactory performance of both the SCPB and SCFM models indicate that turbulent timescale alone is not sufficient to model S_{UR} and T_2. The term S_{UR} can be expressed as: $S_{UR} = \overline{(e_\alpha \sin^2\theta_\alpha + e_\beta \sin^2\theta_\beta + e_\gamma \sin^2\theta_\gamma)}($ (where e_α, e_β and e_γ are the most extensive, intermediate and the most compressive principal fluctuating strain rate tensor (i.e., $e_{ij} = 0.5\,(\partial u_i''/\partial x_j + \partial u_j''/\partial x_i)$) and $\theta_\alpha, \theta_\beta$ and θ_γ are angles between ∇c and eigenvectors associated with e_α, e_β and e_γ, respectively. The SCPB and SCFM models implicitly assume the collinear alignment of ∇c with the eigenvector corresponding to e_γ, which is valid only for passive scalar mixing. For high values of Damköhler number premixed flames, ∇c may locally align with the eigenvector corresponding to e_α (Chakraborty and Swaminathan 2007), which is ignored in these models. Therefore, both SCPB and SCFM models cannot predict the negative values of S_{UR} for small values of u'/S_L where Damköhler number remains high.

In order to avoid the aforementioned limitations of the SCPB and SCFM models, the tangential strain rate term T_2 can alternatively be decomposed as (Katragadda et al. 2011; Sellmann et al. 2017; Varma et al. 2022a):

$$T_2 = \underbrace{\overline{\left(\frac{\partial u_i}{\partial x_i}\right)_s \Sigma_{gen}}}_{D_{FSD}} - \underbrace{\overline{\left(N_i N_j \frac{\partial u_i}{\partial x_j}\right)_s \Sigma_{gen}}}_{N_{FSD}} \qquad (9)$$

Here, the terms D_{FSD} and N_{FSD} denote the effects of dilatation rate and normal strain rate, respectively. The dilatation rate term can be split as $D_{FSD} = D1_{FSD} + D2_{FSD}$ where $D1_{FSD}$ and $D2_{FSD}$ are the mean and fluctuating components, respectively, which are defined as (Katragadda et al. 2011; Sellmann et al. 2017; Varma et al. 2022a):

$$D1_{FSD} = \partial\widetilde{u}_i/\partial x_i |\nabla\overline{c}| \qquad (10i)$$

$$D2_{FSD} = \overline{(\partial u_i/\partial x_i |\nabla c|)} - (\partial\widetilde{u}_i/\partial x_i)|\nabla\overline{c}| \qquad (10ii)$$

The term $D2_{FSD}$ is modelled as (Katragadda et al. 2011; Sellmann et al. 2017; Varma et al. 2022a):

$$D2_{FSD} = (\tau . S_L/\delta_{th})\left[A\left(1-\widetilde{c}\right)^\zeta \left(\Sigma_{gen} - |\nabla\overline{c}|\right)\right] \qquad (11)$$

where $A = B_1/\left(1 + Ka_L\right)^{0.35}$, B_1 and ζ are the model parameters. The model expressions proposed by Varma et al. (2022a) for the components of D_{FSD} and N_{FSD} involving fluctuating quantities previously are summarised in Table 2. In comparison to the model proposed by Varma et al. (2022a), the model parameter B_1 was modified as a function of turbulent Reynolds number Re_L (i.e., $Re_L = \rho_0 \widetilde{k}^2/(\widetilde{\epsilon}\mu_0)$) (Katragadda et al. 2011; Sellmann et al.

Table 2 Models of the fluctuating contributions of D_{FSD} and N_{FSD} (i.e., $D2_{FSD}$ and $N2_{FSD}$) proposed by Varma et al. (2022a) where $g^* = \Gamma \delta_Z / S_L^2$ with Γ being the body force in the direction of mean flame propagation

Quantity	Model expression
$D2_{FSD} = \overline{\left(\partial u_i / \partial x_i \| \nabla c \| \right)} - \partial \widetilde{u}_i / \partial x_i \| \nabla \bar{c} \|$	$D2_{FSD} = \left(\tau . S_L / \delta_{th} \right) \left[A \left(1 - \widetilde{c} \right)^{\zeta} \left(\Sigma_{gen} - \| \nabla \bar{c} \| \right) \right]$ where $A = B_1 / \left(1 + Ka_L \right)^{0.35}, \zeta = -0.3$ and $B_1 = b_1 / \left[erf \left(\left(Re_L + 1.0 \right) / b_2 \right) \right]$ with $b_1 = 1.79 - 0.69 erf(g^* + 0.394)$ for $g^* \geq 0.0$ $b_1 = 0.98 + 0.54 erf(g^* + 1.61)$ for $g^* \leq 0.0$ $b_2 = 17.31 - 13.89 erf(g^* + 1.91)$
$N2_{FSD} = -\overline{\left(N_i N_j \partial u_i'' / \partial x_j \right)}_s \Sigma_{gen}$	$N2_{FSD} = \left(\widetilde{\epsilon} / \widetilde{k} \right) \left[C_1 - \tau C_2 Da_L \right] \Sigma_{gen}$ where $C_1 = B_2 erf \left[\left(Re_L + 1.0 \right) / a_2 \right] . \left(1 - \widetilde{c} \right)^k$ with $B_2 = 3.0$ $k = 4.21 - 1.23 erf(0.89 - 0.35 g^*)$ $a_2 = 23.2 - 17.62 erf(g^* + 1.70)$ and $C_2 = 0.471 B_3 \left[1.0 - \overline{\left(N_k \right)}_s \overline{\left(N_k \right)}_s \right] / \left(1.0 + Ka_L \right)^{0.35}$ with $B_3 = P / erf \left[\left(Re_L + 1.0 \right) / a_3 \right]$ $P = 18.9 - 17.0 erf(g^* + 1.44)$ for $g^* \geq 0.0$ $P = 1.67 + 0.98 erf(g^* + 1.36)$ for $g^* \leq 0.0$ $a_3 = 16.16 - 12.56 erf(g^* + 1.79)$

2017; Varma et al. 2022a). The following expressions of B_1 and ζ are proposed here so that the model given by Eq. (11) can be applied for a range of different values of u'/S_L and l/δ_z:

$$B_1 = 1.8 + 0.75 \text{erf}[\left(Re_L / 60 \right) - 1] \text{ and } \zeta = -0.3 \tag{12}$$

It was demonstrated by Chakraborty and Cant (2013) that most model parameters related to the FSD transport reach asymptotic values for $Re_L \geq 100$. However, it is important to recognise that Eq. (12) is one of the several possibilities of parameterising B_1 such that it assumes an asymptotic value (= 2.55) for $Re_L \rightarrow \infty$ and provides the desired values for moderate values of Re_L corresponding to the DNS data. It is admitted that the parameterisation of B_1 in Eq. (12) (and some of the other model parameters in the following discussion) involves a degree of empiricism but it is not unusual for turbulence and turbulent combustion modelling. Even if these parameterisations are considered to be purely empirical fits to the DNS data, such fits have a value similar to any new experimental or DNS result that shows an effect, which is yet to be analysed. Moreover, these parameterisations are proposed in such a manner that they assume asymptotic values for $Re_L \rightarrow \infty$.

The predictions of D_{FSD} according to Eqs. (10) and (11) (with the model parameter given by Eq. (12)) are compared to the corresponding term extracted from the DNS data in Fig. 10. The predictions using the model proposed by Varma et al. (2022a) are also shown in Fig. 10 for the sake of completeness. Figure 10 shows the model given by Eq. (11)

mostly satisfactorily predict the behaviour of D_{FSD} for all values of u'/S_L and l/δ_z considered in this analysis.

The normal strain rate contribution N_{FSD} can also be split into its respective mean and fluctuating components, i.e., $N_{FSD} = N1_{FSD} + N2_{FSD}$, where $N1_{FSD}$ and $N2_{FSD}$ are defined as (Katragadda et al. 2011; Sellmann et al. 2017; Varma et al. 2022a):

$$N1_{FSD} = -\overline{(N_iN_j)}_s\left(\partial\widetilde{u}_i/\partial x_j\right)\Sigma_{gen} \tag{13i}$$

$$N2_{FSD} = -\overline{\left(N_iN_j\partial u_i''/\partial x_j\right)}_s\Sigma_{gen} \tag{13ii}$$

The predictions of $N1_{FSD}$ with $\overline{(N_iN_j)}_s$ evaluated according to the MCPB and VPDM models are compared to the corresponding term extracted from the DNS data in Fig. 11. It can be seen from Fig. 11 that both MCPB and VPDM models reasonably capture the behaviour of $N1_{FSD}$ extracted from DNS data but their predictions become comparable for high turbulence intensities (e.g., $u'/S_L = 7.5$ and 10.0 cases) for both values of l/δ_z considered in this analysis. However, the VPDM model shows better agreement with DNS data than the MCPB model for $u'/S_L = 1.0$ case for $l/\delta_z = 2.625$, whereas just the opposite behaviour is observed for $u'/S_L = 3.0$ case for $l/\delta_z = 2.625$. For the of l/δ_z values considered in this analysis, the MCPB model tends to overpredict the magnitude of the negative values of $N1_{FSD}$, which is consistent with the underprediction of the magnitude of S_R by the MCPB model shown earlier (see Fig. 8). The observations made from Figs. 8 and 11 reveal that the differences in model predictions for S_R and $N1_{FSD}$ become less sensitive for higher values of l/δ_z.

In order to consider the modelling of the term $N2_{FSD}$ it is worthwhile to express N_{FSD} and T_2 as (Katragadda et al. 2011; Sellmann et al. 2017; Varma et al. 2022a):

$$N2_{FSD} = -\overline{(e_\alpha\cos^2\theta_\alpha + e_\beta\cos^2\theta_\beta + e_\gamma\cos^2\theta_\gamma)|\nabla c|} \tag{14}$$

Here e_α, e_β and e_γ are the most extensive, intermediate and the most compressive principal fluctuating strain rate tensor (i.e., $0.5(\partial u_i''/\partial x_j + \partial u_j''/\partial x_i)$) and $\theta_\alpha, \theta_\beta$ and θ_γ are the angles between ∇c with the eigenvectors associated with e_α, e_β and e_γ, respectively. It has been discussed and demonstrated elsewhere (Chakraborty and Swaminathan 2007; Chakraborty et al. 2011) that ∇c preferentially collinearly aligns with the eigenvectors associated with e_α (i.e., high probability of $|\cos\theta_\alpha| \approx 1.0$) under the dominance of the strain rate induced by flame normal acceleration arising from heat release over turbulent straining. By contrast, ∇c demonstrates preferential collinear alignment with the eigenvectors associated with e_γ (i.e., high probability of $|\cos\theta_\gamma| \approx 1.0$) as a result of the dominance of turbulent straining over the strain rate induced by flame normal acceleration arising from heat release (Chakraborty and Swaminathan 2007; Chakraborty et al. 2011). The high probability of obtaining $|\cos\theta_\alpha| \approx 1.0$ is obtained for $\tau Da \gg 1$ (Chakraborty and Swaminathan 2007; Chakraborty et al. 2011), which leads to negative values of $N2_{FSD}$ (and in turn promotes negative values of N_{FSD} and T_2). By contrast, high probability of obtaining $|\cos\theta_\gamma| \approx 1.0$ is obtained for $\tau Da < 1$, which gives rise to positive values of $N2_{FSD}$ (and in turn promotes positive values of N_{FSD} and T_2). For a given value of l/δ_z, an increase in u'/S_L leads to a reduction in Da and therefore, the likelihood of obtaining positive values of $N2_{FSD}$ increases with increasing turbulence intensity, which can be substantiated from Fig. 12 where the variations of $N2_{FSD} \times \delta_z^2/S_L$ with $\widetilde{c}$ for all cases considered here are shown. It can indeed be seen from Fig. 12 that $N2_{FSD}$ assumes negative values throughout
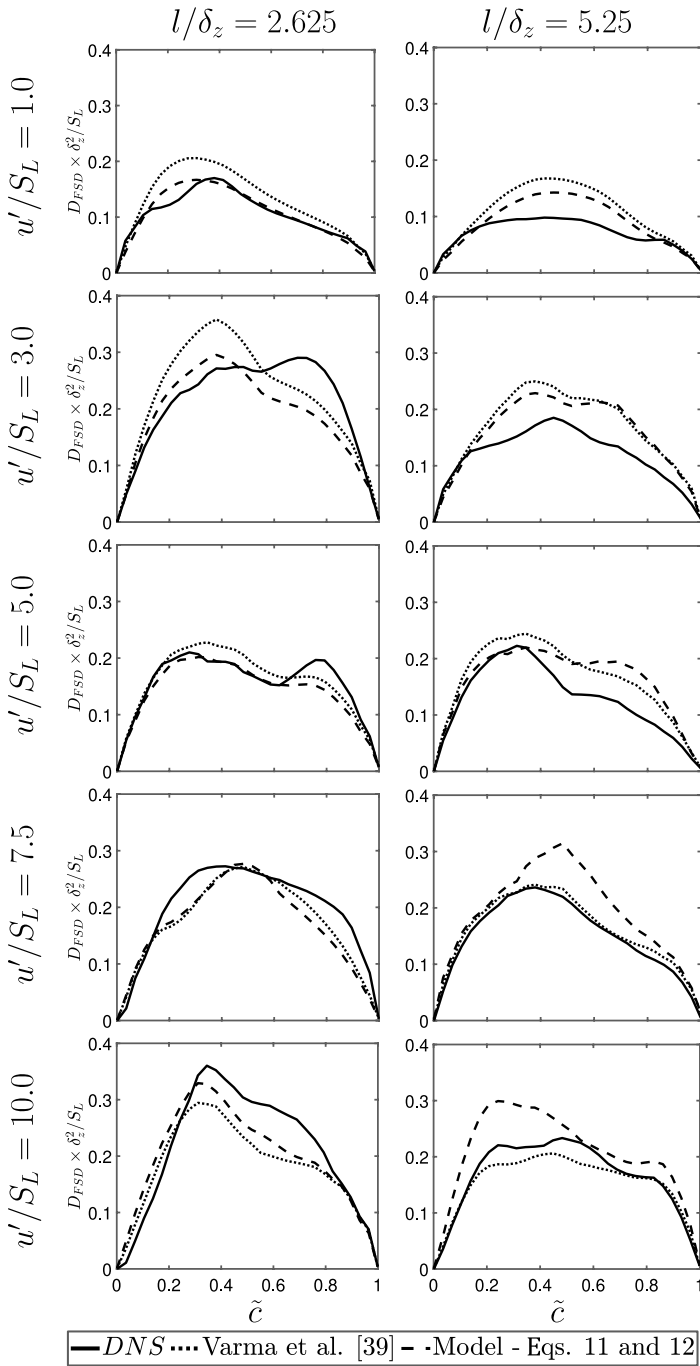
Fig. 10 Variation of $D_{FSD} \times \delta_z^2/S_L$ with $\tilde{c}$ for $l/\delta_z = 2.625$ (left) and 5.25 (right) along with the predictions using the closures given by Eqs. (11) and (12) for $u'/S_L = 1.0$, 3.0, 5.0, 7.5 and 10.0 (1st–5th row). Also shown are the prediction using the closures proposed by Varma et al. (2022a)
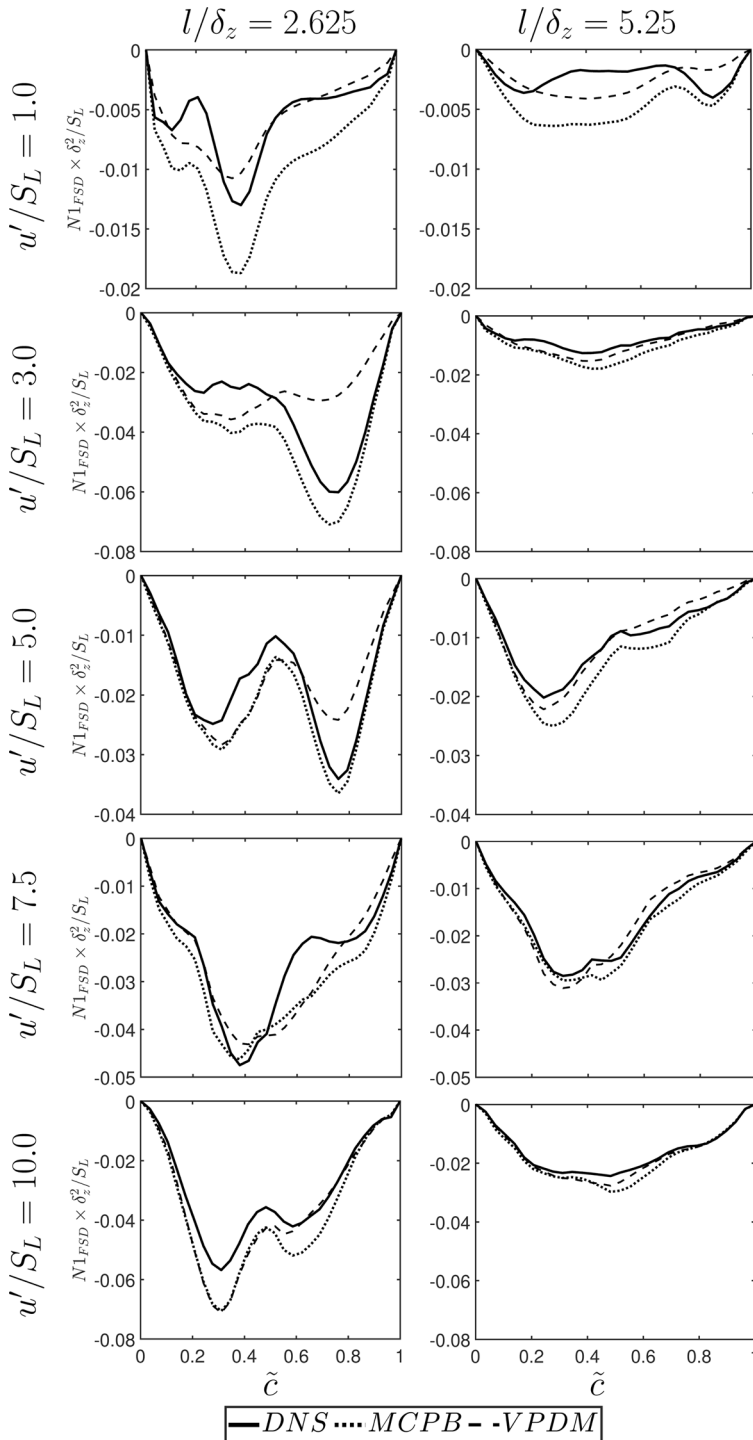
Fig. 11 Variation of $N1_{FSD} \times \delta_z^2/S_L$ with $\widetilde{c}$ for $l/\delta_z = 2.625$ (left) and 5.25 (right) along with the predictions of the MCPB and VPDM model for $u'/S_L = 1.0, 3.0, 5.0, 7.5$ and 10.0 (1st–5th row)

the flame brush for small values of turbulence intensity (e.g., $u'/S_L = 1.0$ and 3.0), whereas for large turbulence intensities (e.g., $u'/S_L = 7.5$ and 10.0) $N2_{FSD}$ assumes positive values towards the unburned gas side of the flame brush where the effects of heat release are weak but this term becomes negative from the middle to the burned gas side of the flame brush where the effects of strain rate arising from flame normal acceleration remain strong. It is also worth noting that for a given value of u'/S_L, an increase in l/δ_z leads to an increase in Damköhler number Da and thus the extent of collinear alignment of ∇c with the eigenvector associated with e_α (e_γ) is greater (smaller) in the $l/\delta_z = 5.25$ cases than in the $l/\delta_z = 2.625$ cases. This is reflected in the higher (smaller) of the propensity negative (positive) contribution of $N2_{FSD}$ for higher l/δ_z case for a given value of u'/S_L, which can also be confirmed from Fig. 12.

The foregoing discussion suggests that the competition between the strain rate induced by flame normal acceleration and turbulent straining, and the alignment characteristics of ∇c need to be addressed to model N_{FSD}. This is addressed by the following model expression in previous studies (Katragadda et al. 2011; Sellmann et al. 2017; Varma et al. 2022a):

$$N2_{FSD} = \left(\widetilde{\epsilon}/\widetilde{k}\right)\left[C_1 - \tau C_2 Da_L\right]\Sigma_{gen} \tag{15}$$

where $Da_L = \widetilde{k}S_L/\widetilde{\epsilon}\delta_{th}$ is the local Damköhler number. For small values of Damköhler number ∇c preferentially aligns with the eigenvector associated with e_γ due to the dominance of turbulent straining over the effects of heat release, which is modelled as $\left(\widetilde{\epsilon}/\widetilde{k}\right)C_1\Sigma_{gen}$ in Eq. (15). For high Damköhler numbers, heat release effects dominate over the turbulent straining, which leads to the preferential alignment of ∇c with the eigenvector associated with e_α. This aspect is accounted for by $-\tau C_2\Sigma_{gen}S_L/\delta_{th}$ in Eq. (15). In the present analysis, C_1 and C_2 have been revised in comparison to the previous expressions proposed by Varma et al. (2022a) in the following manner to account for l/δ_z dependences which have been embedded in Re_L:

$$C_1 = [0.25 + 2.6erf(Re_L/50)]\left(1 - \widetilde{c}\right)^{3.2} \tag{16}$$

$$C_2 = 0.471\{0.2 + erfc\left[(Re_L - 42)/50\right]\}\left[1.0 - \overline{(N_k)}_s\overline{(N_k)}_s\right]/\left(1.0 + Ka_L\right)^{0.35} \tag{17}$$

It can be seen from Fig. 12 that the predictions of the model given by Eq. (15) with model parameters according to Eqs. (16) and (17) remain in satisfactory agreement with $N2_{FSD}$ extracted from DNS data including its negative value for small values of turbulence intensity (e.g., $u'/S_L = 1.0$ and 3.0) and the transition from positive to negative values of $N2_{FSD}$ for large turbulence intensities (e.g., $u'/S_L = 7.5$ and 10.0). It can also be observed from Fig. 12 that the modifications to the closures proposed by Varma et al. (2022a) have resulted in significantly improved predictions of the $N2_{FSD}$ term.

A combination of the MCPB model for $N1_{FSD}$ with Eqs. (10), (11) and (15–17) for $D1_{FSD}$, $D2_{FSD}$ and $N2_{FSD}$ respectively yield the following model for the strain rate term T_2:
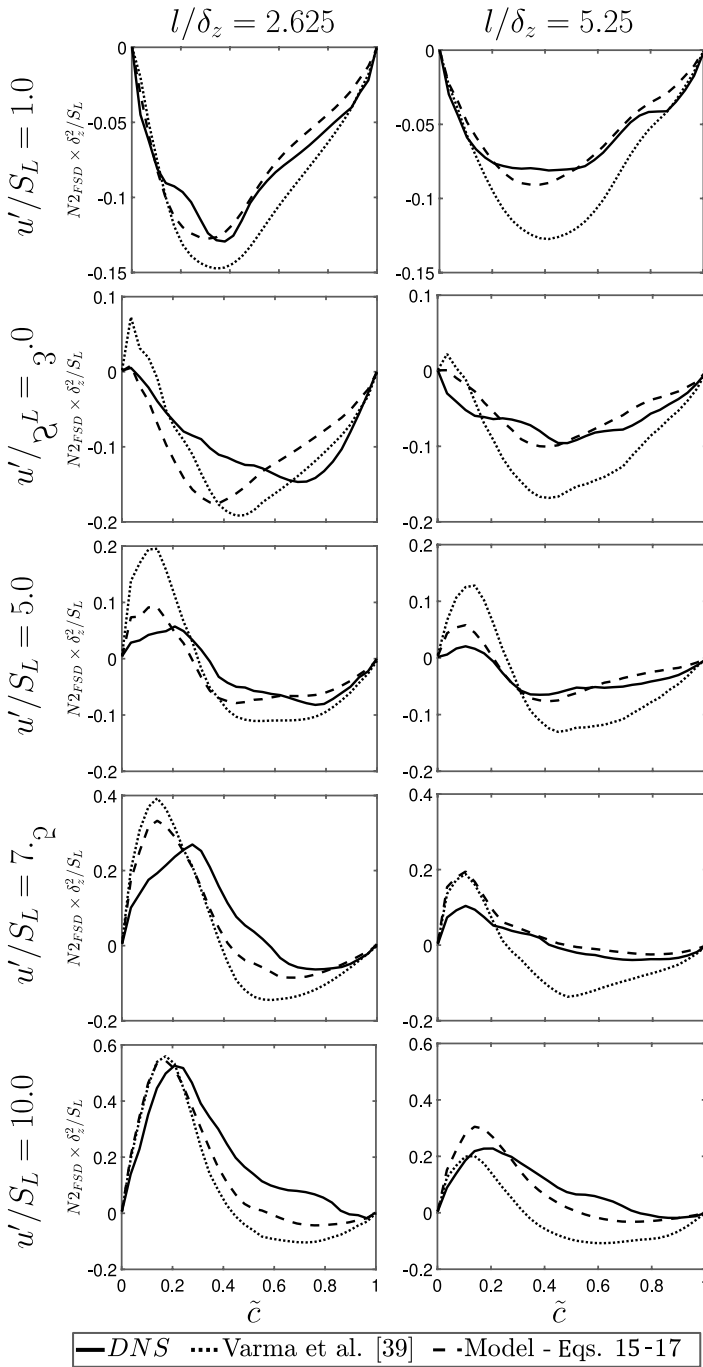
Fig. 12 Variation of $N2_{FSD} \times \delta_z^2/S_L$ with $\tilde{c}$ for $l/\delta_z = 2.625$ (left) and 5.25 (right) along with the predictions of the model given by Eqs. (15–17) for $u'/S_L = 1.0$, 3.0, 5.0, 7.5 and 10.0 (1st–5th row). Also shown are the predictions using the closures proposed by Varma et al. (2022a)

$$T_2 = \frac{\partial \widetilde{u}_i}{\partial x_i}|\nabla \overline{c}| + \frac{\tau . S_L}{\delta_{th}}\left[A\left(1 - \widetilde{c}\right)^\zeta \left(\Sigma_{gen} - |\nabla \overline{c}|\right)\right] - \overline{\left(N_i\right)_s \left(N_j\right)_s}$$
$$\frac{\partial \widetilde{u}_i}{\partial x_j}\Sigma_{gen} - \left(\delta_{ij}/3\right)\left[1 - \overline{\left(N_k\right)_s \left(N_k\right)_s}\right] \tag{18}$$
$$\frac{\partial \widetilde{u}_i}{\partial x_j}\Sigma_{gen} + \frac{\widetilde{\epsilon}}{k}\left[C_1 - \tau C_2 Da_L\right]\Sigma_{gen}$$

The predictions of Eq. (18) are compared to the predictions of the CPB (MCPB + SCPB) and CFM (VPDM + SCFM) models in Fig. 13 along with the T_2 term extracted from DNS data and the predictions of T_2 according to the closures proposed by Varma et al. (2022a). Figures 13 shows that Eq. (18) agrees better with the DNS data than the CPB and CFM models for $u'/S_L \geq 5.0$ cases for both values of l/δ_z but Eq. (18) overpredicts T_2 for $l/\delta_z = 5.25$ cases for $u'/S_L = 1.0$ and 3.0, whereas an underprediction is obtained for the $l/\delta_z = 2.625$ case with $u'/S_L = 3.0$. Despite these discrepancies between the predictions of Eq. (18) and DNS data, the performance of Eq. (18) remains better than the CPB and CFM models. It is worth noting that Eq. (18) takes care about the competition between the strain rates due to turbulence and flame normal acceleration through the model for $N2_{FSD}$ (see Eq. (15)) in response to the variations of Damköhler number, which is missing in the CPB and CFM models. Thus, Eq. (18) performs better than the SPB and SCFM models for a broad range of values of u'/S_L and l/δ_z. Figure 13 also shows that Eq. (18) gives better predictions of the T_2 term in comparison to the closures proposed by Varma et al. (2022a) especially for higher u'/S_L values for both length scales. This can be attributed to the use of forced turbulence in the present study compared to decaying turbulence used by Varma et al. (2022a), which results in higher turbulence levels at the time of extraction of statistics in the present study for all initial u'/S_L cases compared to the analysis by Varma et al. (2022a).

4.5 Modelling of the Combined Propagation and Curvature Terms ($T_3 + T_4$)

The curvature term T_4 can be expressed as: $T_4 = 2\overline{\left[\left(S_r + S_n\right)\kappa_m\right]_s}\Sigma_{gen} - 4\overline{\left(D\kappa_m^2\right)_s}\Sigma_{gen}$ (Chakraborty and Cant 2011; Katragadda et al. 2014b) where reaction and normal diffusion components of displacement speed are defined as: $S_r = \dot{\omega}/\rho|\nabla c|$ and $S_n = \vec{N} \bullet (\rho D\vec{N} \bullet \nabla c)/\rho|\nabla c|$ (Peters et al. 1998; Echekki and Chen 1999). For high values of Karlovitz number (i.e., $Ka \gg 1$) the negative contribution of $\{-4\overline{\left(D\kappa_m^2\right)_s}\Sigma_{gen}\}$ becomes the dominant term, whereas the contribution of $2\overline{\left[\left(S_r + S_n\right)\kappa_m\right]_s}\Sigma_{gen}$ remains dominant for small and moderate values of Ka (i.e., $Ka < 1$ and $Ka \sim 1.0$). The qualitative behaviour of $2\overline{\left[\left(S_r + S_n\right)\kappa_m\right]_s}\Sigma_{gen}$ is determined by the behaviour of $\overline{\left(\kappa_m\right)_s}$ because $\left(S_r + S_n\right)$ remains predominantly positive and Σ_{gen} is a positive semi-definite quantity (i.e., $\Sigma_{gen} \geq 0$). It was demonstrated earlier (Chakraborty and Cant 2011, 2013; Katragadda et al. 2014b) that $\overline{\left(\kappa_m\right)_s}$ assumes positive (negative) values towards the unburned (burned) gas side of the flame brush and the same qualitative behaviour has been observed here but not shown here for brevity. The aforementioned behaviour of $\overline{\left(\kappa_m\right)_s}$ leads to positive (negative) values of $2\overline{\left[\left(S_r + S_n\right)\kappa_m\right]_s}\Sigma_{gen}$ towards the unburned (burned) gas side of the flame brush. A decrease in l/δ_z for a given value of u'/S_L gives rise to an increase in Ka. Thus, the negative contribution of $\{-4\overline{\left(D\kappa_m^2\right)_s}\Sigma_{gen}\}$ is more likely to dominate over $2\overline{\left[\left(S_r + S_n\right)\kappa_m\right]_s}\Sigma_{gen}$ for smaller values of l/δ_z (due to an increase in Karlovitz number with a decrease in l/δ_z) according to the scaling argument by Peters (2000) and it can indeed be seen from Fig. 5 that the
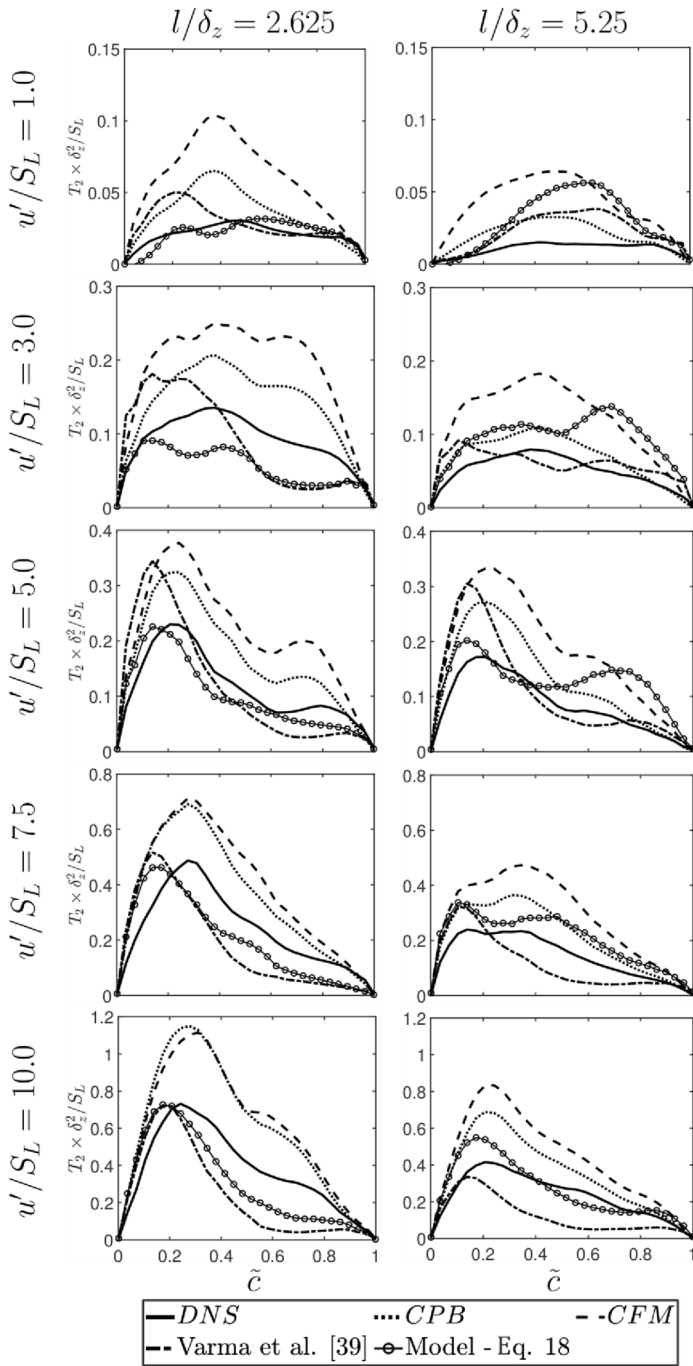
Fig. 13 Variation of $T_2 \times \delta_z^2/S_L$ with $\widetilde{c}$ for $l/\delta_z = 2.625$ (left) and 5.25 (right) along with the predictions of the CPB, CFM models and the model given by Eq. (18) for $u'/S_L = 1.0, 3.0, 5.0, 7.5$ and 10.0 (1st–5th row). Also shown are the predictions using the closures given by Varma et al. (2022a)

magnitude of the negative contribution of T_4 is higher for smaller values of l/δ_z. Moreover, Karlovitz number increases with increasing u'/S_L, which also acts to increase the range of curvature values which gives rise to the increase in the magnitude of the negative contribution of $\{-4\overline{\left(D\kappa_m^2\right)_s}\Sigma_{gen}\}$. Accordingly it can be seen from Fig. 14 that $(T_3 + T_4)$ assumes positive values towards the unburned gas and negative values towards the burned gas side of the flame brush for $u'/S_L \leq 5.0$ but the net contribution of these terms assumes predominantly negative values throughout the flame brush for $u'/S_L = 7.5$ and 10.0.

The curvature and propagation terms are usually modelled together due to their dependence on the displacement speed S_d but the behaviour of $(T_3 + T_4)$ is principally determined by the curvature term as the magnitude of the propagation term T_3 remains much smaller than T_4. The term $(T_3 + T_4)$ is usually modelled together as (Hun and Huh 2008; Chakraborty and Cant 2011, 2013; Sellmann et al. 2017; Varma et al. 2022a):

$$(T_3 + T_4) = -\frac{\partial}{\partial x_i}\left[\frac{\rho_0 S_L}{\overline{\rho}}\overline{(N_i)_s}\Sigma_{gen}\right] + \frac{\rho_0 S_L}{\overline{\rho}}\frac{\partial\overline{(N_i)_s}}{\partial x_i}\Sigma_{gen} - \beta_0\alpha_N\frac{(\overline{c} - c_{cp})S_L\Sigma_{gen}^2}{\overline{c}(1 - \overline{c})} \quad (19)$$

The last term on the right-hand side of Eq. (19) denotes the fluctuating component of the combined propagation and curvature term where β_0 and c_{cp} are model parameters, and α_N represents an orientation factor (resolution factor) in terms of RANS (LES) which is expressed as $\alpha_N = 1 - \overline{(N_k)_s}\overline{(N_k)_s}$ and thus becomes zero under fully resolved condition causing the last term to vanish (Fureby 2005; Hawkes and Cant 2000; Jenkins and Cant 1999; Katragadda et al. 2014b). Previous analyses (Hun and Huh 2008; Chakraborty and Cant 2011, 2013; Sellmann et al. 2017; Varma et al. 2022a) suggested $\beta_0 = 8.0$ and $c_{cp} = 0.35$ for unity Lewis number flames. The predictions of Eq. (19) are compared to $(T_3 + T_4)$ extracted from DNS data in Fig. 14. It can be seen from Fig. 14 that the $(T_3 + T_4)$ is adequately captured by Eq. (19) for $\beta_0 = 8.0$ and $c_{cp} = 0.35$ for both values of l/δ_z for $u'/S_L \leq 5.0$ where $(T_3 + T_4)$ assumes positive values towards the unburned gas and negative values towards the burned gas side of the flame brush. However, Eq. (19) for $\beta_0 = 8.0$ and $c_{cp} = 0.35$ predicts positive values towards the unburned gas side of the flame brush for high turbulence intensities (e.g., $u'/S_L = 7.5$ and 10.0) but DNS data shows negative values throughout the flame brush. In order to capture negative values of $(T_3 + T_4)$ throughout the flame brush for $u'/S_L = 7.5$ and 10.0, the parameter c_{cp} is altered in this analysis in the following manner:

$$c_{cp} = 0.01 + erfc[(Re_L + 6)/36] \quad (20)$$

The predictions of Eq. (19) with $\beta_0 = 8.0$ and c_{cp} according to Eq. (20) are also shown in Fig. 14, which shows that this model captures the behaviour of $(T_3 + T_4)$ throughout the flame brush for all cases considered here.

4.6 Mean Reaction Rate Closure Using Generalised FSD

The variations of $\overline{\dot{\omega}}$ and $\overline{\dot{\omega}} + \overline{\nabla.(\rho D\nabla c)}$ with $\tilde{c}$ for all cases considered here are shown in Fig. 15. It can be seen from Fig. 15 that there is a good level of agreement between $\overline{\dot{\omega}}$ and $\overline{\dot{\omega}} + \overline{\nabla.(\rho D\nabla c)}$, which shows that the contribution of the mean molecular diffusion rate in statistically planar flames is much smaller than the mean reaction rate and hence
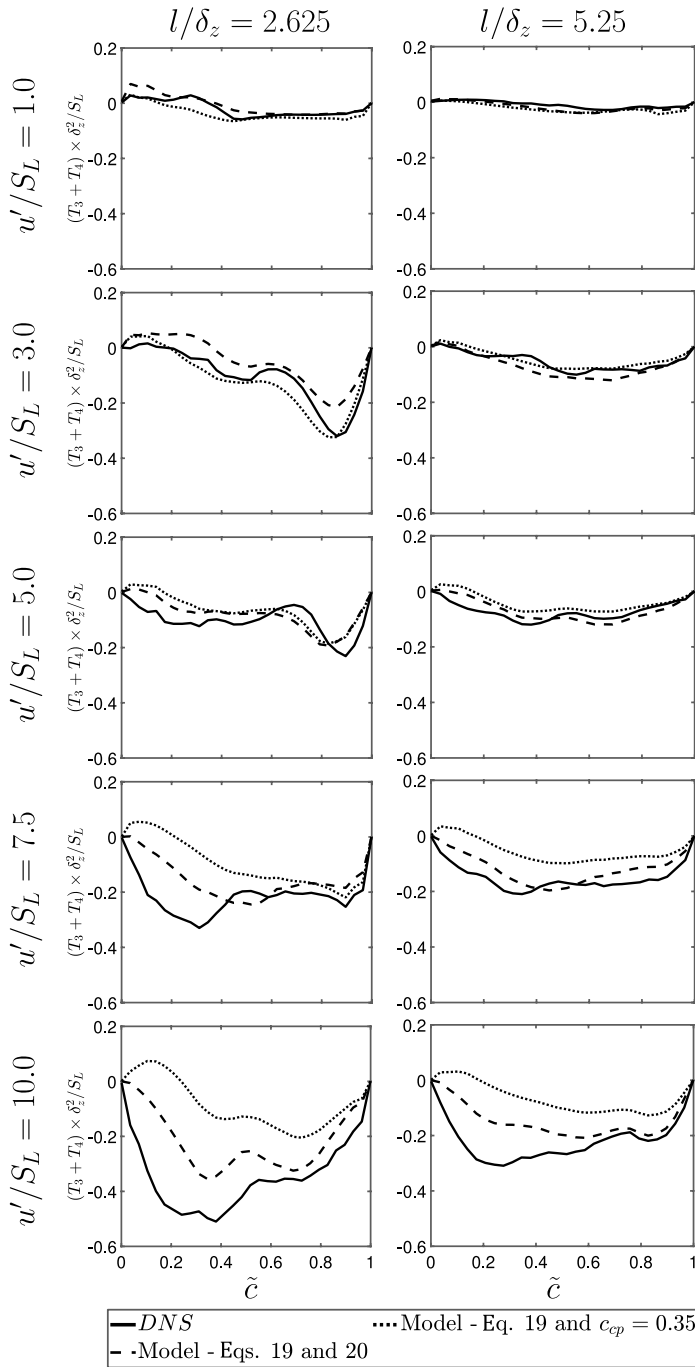
Fig. 14 Variation of the combined propagation and curvature term $(T_3 + T_4) \times \delta_z^2/S_L$ with $\tilde{c}$ for $l/\delta_z = 2.625$ (left) and 5.25 (right) along with the predictions of the model expressions given by Eq. (19) with $c_p = 0.35$ and c_p given by Eq. (20) for $u'/S_L = 1.0$, 3.0, 5.0, 7.5 and 10.0 (1st–5th row)
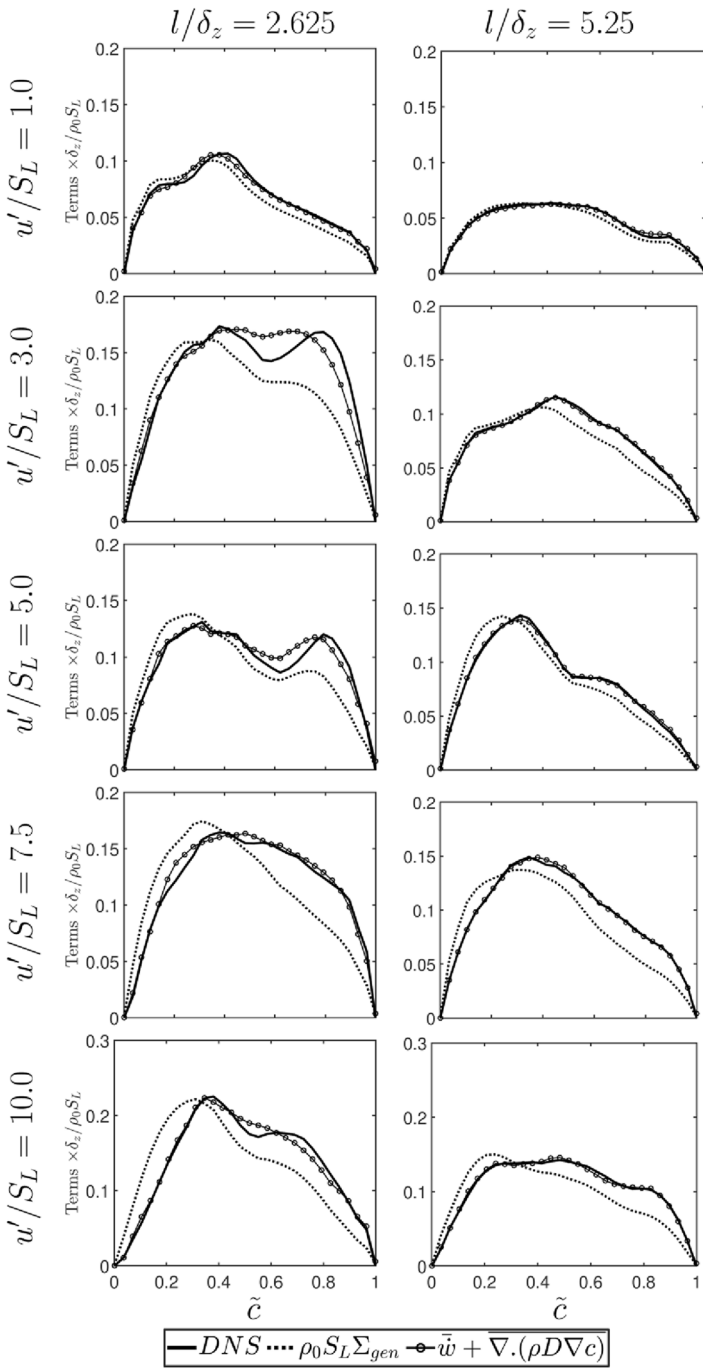
Fig. 15 Variation of $\overline{\dot{\omega}} \times \delta_Z/\rho_0 S_L$ and $\overline{\dot{\omega} + \nabla.(\rho D \nabla c)} \times \delta_z/\rho_0 S_L$ with $\tilde{c}$ for $l/\delta_z = 2.625$ (left) and 5.25 (right) along with the predictions of the model given by $\overline{(\rho S_d)}_s \approx \rho_0 S_L$ for $u'/S_L = 1.0, 3.0, 5.0, 7.5$ and 10.0 (1st–5th row)

$\overline{\dot{\omega}} \approx \overline{(\rho S_d)}_s \Sigma_{gen}$ holds in the context of RANS simulations. For unity Lewis number flames, the surface-averaged density-weighted displacement speed is usually modelled as $\overline{(\rho S_d)}_s \approx \rho_0 S_L$ (Hawkes and Cant 2000, 2001) although this approximation may not be valid, especially for the thin reaction zones regime flames (Sabelnikov et al. 2017). Thus, the model for mean reaction rate may be expressed as $\overline{\dot{\omega}} = \rho_0 S_L \Sigma_{gen}$. It can further be seen from Fig. 15 that $\rho_0 S_L \Sigma_{gen}$ satisfactorily captures the variation of $\overline{\dot{\omega}}$ across the flame brush but $\rho_0 S_L \Sigma_{gen}$ underpredicts the magnitude of $\overline{\dot{\omega}}$ towards the product side of the flame brush for all cases.

It is worth noting that the quantity $\overline{\dot{\omega}} + \overline{\nabla.(\rho D \nabla c)}$, by definition, equals to $\overline{(\rho S_d)}_s \Sigma_{gen}$ and thus a comparison between $\overline{(\rho S_d)}_s \Sigma_{gen}$ and $\rho_0 S_L \Sigma_{gen}$ in Fig. 15 indicates that the magnitude of $\overline{(\rho S_d)}_s$ remains close to $\rho_0 S_L$ for the cases considered here. Thus, the discrepancy between $\overline{\dot{\omega}} + \overline{\nabla.(\rho D \nabla c)}$ (i.e., $\overline{\dot{\omega}}$ due to $\overline{\dot{\omega}} \gg \overline{\nabla.(\rho D \nabla c)}$) and $\rho_0 S_L \Sigma_{gen}$ originates due to the approximation of $\overline{(\rho S_d)}_s \approx \rho_0 S_L$ and a better representation of $\overline{(\rho S_d)}_s$ is likely to provide an improved prediction of the mean reaction rate. the discrepancy between $\rho_0 S_L \Sigma_{gen}$ and $\overline{\dot{\omega}}$ originates due to the approximation of $\overline{(\rho S_d)}_s \approx \rho_0 S_L$ and a better representation of $\overline{(\rho S_d)}_s$ is likely to provide an improved prediction of the mean reaction rate.

5 Conclusions

The effects of both turbulence intensity u'/S_L and integral length scale to flame thickness ratio l/δ_z on the statistical behaviours of FSD and its transport have been evaluated using a DNS database of three-dimensional statistically planar turbulent premixed flames. In contrast to several previous analyses (Trouvé and Poinsot 1994; Hawkes and Cant 2000, 2001; Chakraborty and Cant 2007, 2009a, 2011, 2013; Hun and Huh 2008; Katragadda et al. 2011, 2014a, b; Papapostolou et al. 2019; Varma et al. 2022a), the current study assesses the performances of the models for different unclosed terms in the FSD transport equation in response to the variations of both u'/S_L and l/δ_z. The main findings are summarised below:

- It has been found that the peak magnitudes of the FSD and the terms of the FSD transport term decrease with an increase in length scale ratio.
- The turbulent burning velocity and flame surface area assume greater values for the higher values of length scale ratio l/δ_z for a given value of u'/S_L. Both turbulent burning velocity and flame surface area increase with increasing u'/S_L before the bending behaviour at high values of u'/S_L.
- The flame brush thickness and flame wrinkling increase with an increase in l/δ_z for a given value of u'/S_L. However, the qualitative behaviours of the unclosed terms in the FSD transport equation remain unchanged by the length scale ratio and in all cases the tangential strain rate term T_2 acts as a leading order source and the curvature term T_4 remains the major sink term towards the burned gas of the flame brush.
- A decrease in l/δ_z for a given value of u'/S_L leads to a decrease in Damköhler number and an increase in Karlovitz number. This has an implication on the alignment of reactive scalar gradient with local strain rate eigenvectors. Therefore, the existing models for the tangential strain rate term, which do not explicitly account for the alignment of reactive scalar gradient with local strain rate eigenvectors in response to the changes

in Damköhler number, have been found to be inadequate. An alternative model for the tangential strain rate term T_2, which explicitly considers the alignment of ∇c with local strain rate eigendirections and the competition between turbulent straining and chemical timescales, has been shown to be more successful in capturing the behaviour obtained from DNS data.

- It has been found that an existing model for the turbulent flux of the FSD, which accounts for both gradient and counter-gradient behaviour, does not need any major modifications due to l/δ_z variation. The nature of turbulent transport is determined by relative strengths of turbulent velocity fluctuation and velocity jump across the flame, which is not directly affected by l/δ_z.

- According to scaling argument by Peters (2000), the curvature term is expected to show greater likelihood of negative values for higher Karlovitz number and accordingly larger magnitudes of the curvature term are obtained for smaller (higher) value of l/δ_z (u'/S_L) for a given value of u'/S_L (l/δ_z). As a result, the combined propagation and curvature term $\left(T_3 + T_4\right)$ showed predominantly negative contribution for high Karlovitz number values, which needed modification to an existing model.

- The FSD based mean reaction rate closure mostly works satisfactorily irrespective the value of l/δ_z but underpredicts the magnitude of $\overline{\dot{\omega}}$ for all cases towards the product side of the flame brush due to inaccuracies involved in modelling surface-averaged density-weighted displacement speed.

It is worth noting that the current analysis has been conducted with simple chemistry for the sake of a detailed parametric analysis. Although previous analyses (Papapostolou et al. 2019; Luca et al. 2019) revealed no major differences in the qualitative behaviours of the unclosed terms of the FSD transport equation between simple and detailed chemistry, future analyses need to include the effects of detailed chemistry for comprehensive validation of the models proposed in this analysis. The turbulent Reynolds number $Re_t = \rho_0 k^2 / \mu_0 \varepsilon$ ranges from 12.5 (for case A2) to 250 (case E1) for the DNS database considered here. It is worth noting that most laboratory scale experiments have Re_t values of the order of 100. The range of u'/S_L and l/δ_z considered here is comparable to previous studies by other authors (Trouvé and Poinsot 1994; Boger et al. 1998; Charlette et al. 2002; Hun and Huh 2008; Reddy and Abraham 2012) which contributed to the FSD transport modelling. The FSD/wrinkling models which have been either proposed or recommended based on a priori DNS analysis (Boger et al. 1998; Charlette et al. 2002; Fureby 2005; Chakraborty and Cant 2009a) for moderate turbulent Reynolds numbers have been found to work well based on a posteriori analyses (Ma et al. 2013, 2014; Klein et al. 2016). However, further analyses for higher values of Re_t will be needed to confirm the current findings. Finally, these models need to be implemented in actual RANS simulations of an experimental configuration for the purpose of a posteriori assessment of the closures of the unclosed terms.

Author Contribution NC and UA conceptualised the analysis. AV and NC wrote the original version of the paper. AV did the simulations and prepared the figures. NC and UA reviewed the manuscript. NC and UA supervised AV.

Declarations

Conflict of interest The authors declare that they have no conflict of interest.

Ethical Approval No specific ethical approval is required for this work.

Informed Consent Not applicable for this work.

References

Abu-Orf, G.M., Cant, R.S.: A turbulent reaction rate model for premixed turbulent combustion in Spark-Ignition engines. Combust. Flame **122**, 233–252 (2000)

Ahmed, U., Chakraborty, N., Klein, M.: Insights into the bending effect in premixed turbulent combustion using the Flame Surface Density transport. Combust. Sci. Technol. **191**, 898–920 (2019)

Ahmed, U., Chakraborty, N., Klein, M.: Assessment of Bray Moss Libby formulation for premixed flame-wall interaction within turbulent boundary layers: influence of flow configuration. Combust. Flame **233**, 111575 (2021)

Batchelor, G.K., Townsend, A.: Decay of turbulence in the final period. Proc. r. Soc. A **194**(1039), 527–543 (1948)

Berger, L., Attili, A., Pitsch, H.: Synergistic interactions of thermodiffusive instabilities and turbulence in lean hydrogen flames. Combust. Flame **244**, 112254 (2022)

Boger, M., Veynante, D., Boughanem, H., Trouvé, A.: Direct numerical simulation analysis of flame surface density concept for Large Eddy Simulation of turbulent premixed combustion. Proc. Combust. Inst. **27**, 917–925 (1998)

Bray, K.N.C.: Turbulent flows with premixed reactants. In: Libby, P.A., Williams, F.A. (eds.) Turbulent Reacting Flows, pp. 115–183. Springer Verlag, Berlin Heidelburg, New York (1980)

Bray, K.N.C., Libby, P.A., Moss, J.B.: Unified modeling approach for premixed turbulent combustion—part i: general formulation. Combust. Flame **61**(1), 87–102 (1985)

Bray, K.N.C.: Studies of turbulent burning velocity. Proc. r. Soc. Lond. A **431**, 315–335 (1990)

Bray, K., Champion, M., Libby, P.A., Swaminathan, N.: Scalar dissipation and mean reaction rates in premixed turbulent combustion. Combust. Flame **158**, 2017–2022 (2011)

Cant, R.S., Bray, K.N.C.: Strained laminar flamelet calculations of premixed turbulent combustion in a closed vessel. Proc. Combust. Inst. **22**, 791–799 (1988)

Cant, R.S., Bray, K.N.C.: A theoretical model of premixed turbulent combustion in closed vessels. Combust. Flame **76**, 243–263 (1989)

Cant, R.S., Pope, S.B., Bray, K.N.C.: Modelling of flamelet surface to volume ratio in turbulent premixed combustion. Proc. Combust. Inst. **27**, 809–815 (1990)

Candel, S.M., Poinsot, T.J.: Flame stretch and the balance equation for the flame area. Combust. Sci. Technol. **70**, 1–15 (1990)

Candel, S., Venante, V., Lacas, F., Maistret, E., Darabhia, N., Poinsot, T.: Coherent flamelet model: applications and recent extensions. In: Larrouturou, B.E. (ed.) Recent Advances in Combustion Modelling, pp. 19–64. World Scientific, Singapore (1990)

Chakraborty, N., Cant, R.S.: Statistical behaviour and modelling of flame normal vector in turbulent premixed flames. Num. Heat Trans. A **50**, 623–643 (2006)

Chakraborty, N., Cant, R.S.: A priori analysis of the curvature and propagation terms of the flame surface density transport equation for large eddy simulation. Phys. Fluids **19**, 105101 (2007)

Chakraborty, N., Swaminathan, N.: Influence of Damköhler number on turbulence-scalar interaction in premixed flames, part i: physical insight. Phys. Fluids **19**, 045103 (2007)

Chakraborty, N., Klein, M.: A-priori direct numerical simulation assessment of algebraic flame surface density models for turbulent premixed flames in the context of large eddy simulation. Phys. Fluids **20**, 085108 (2008)

Chakraborty, N., Cant, R.S.: Direct numerical simulation analysis of the flame surface density transport equation in the context of large eddy simulation. Proc. Combust. Inst. **32**, 1445–1453 (2009a)

Chakraborty, N., Cant, R.S.: Effects of Lewis number on scalar transport in turbulent premixed flames. Phys. Fluids **21**, 035110 (2009b)

Chakraborty, N., Cant, R.S.: Effects of Lewis number on turbulent scalar transport and its modelling in turbulent premixed flames. Combust. Flame **156**, 1427–1444 (2009c)

Chakraborty, N., Cant, R.S.: Physical insight and modelling for Lewis number effects on turbulent heat and mass transport in turbulent premixed flames. Num. Heat Trans. A **55**(8), 762–779 (2009d)

Chakraborty, N., Cant, R.S.: Effects of Lewis number on flame surface density transport in turbulent premixed combustion. Combust. Flame **158**, 1768–1787 (2011)

Chakraborty, N., Swaminathan, N.: Effects of Lewis number on scalar variance transport in turbulent premixed flames. Flow Turb. Combust. **87**, 261–292 (2011)

Chakraborty, N., Champion, M., Mura, A., Swaminathan, N.: Scalar dissipation rate approach to reaction rate closure, Turbulent premixed flame. In: Swaminathan, N., Bray, K.N.C. (Eds), 1st Edition. Cambridge University Press, Cambridge, UK, pp. 74–102 (2011)

Chakraborty, N., Cant, R.S.: Turbulent reynolds number dependence of flame Surface Density transport in the context of Reynolds averaged Navier Stokes simulations. Proc. Combust. Inst. **34**, 1347–1356 (2013)

Chakraborty, N., Alwazzan, D., Klein, M., Cant, R.S.: On the validity of Damköhler's first hypothesis in turbulent Bunsen burner flames: a computational analysis. Proc. Combust. Inst. **37**, 2231–2239 (2019)

Charlette, F., Meneveau, C., Veynante, D.: A power law wrinkling model for LES of premixed turbulent combustion, part I: non dynamic formulation and initial tests. Combust. Flame **131**, 159–181 (2002)

Duclos, J.M., Veynante, D., Poinsot, T.: A comparison of flamelet models for turbulent premixed combustion. Combust. Flame. **95**, 101–107 (1993)

Echekki, T., and Chen, J.H.: Analysis of the contribution of curvature to premixed flame propagation. Combust. Flame. **118**, 303–311 (1999)

Fureby, C.: A fractal flame wrinkling large eddy simulation model for premixed turbulent combustion. Proc. Combust. Inst. **30**, 593–601 (2005)

Gouldin, F.C., Bray, K.N.C., Chen, J.: Chemical closure model for fractal flamelets. Combust. Flame **77**, 241–259 (1989)

Hawkes, E.R., Cant, R.S.: A flame surface density approach to large eddy simulation of premixed turbulent combustion. Proc. Combust. Inst. **28**, 51–58 (2000)

Hawkes, E.R., Cant, R.S.: Implications of a flame surface density approach to large eddy simulation of premixed turbulent combustion. Combust. Flame **126**, 1617–1629 (2001)

Hernandez-Perez, F.E., Yuen, F.T.C., Groth, C.P.T., Gülder, Ö.L.: LES of a laboratory-scale turbulent premixed Bunsen flame using FSD, PCM-FPI and thickened flame models. Proc. Combust. Inst. **33**, 1365–1371 (2011)

Hun, I., Huh, K.Y.: Roles of displacement speed on evolution of flame surface density for different turbulent intensities and Lewis numbers in turbulent premixed combustion. Combust. Flame **152**, 194–205 (2008)

Jenkins, K.W., Cant, R.S.: Direct numerical simulation of turbulent flame Kernels. Recent Adv. DNS LES Fluid Mech. Its Appl. **54**, 191–202 (1999)

Katragadda, M., Malkeson, S.P., Chakraborty, N.: Modelling of the tangential strain rate term of the flame surface density transport equation in the context of Reynolds averaged Navier Stokes simulation. Proc. Combust. Inst. **33**, 1429–1437 (2011)

Katragadda, M., Gao, Y., Chakraborty, N.: Modelling of the strain rate contribution to the FSD transport for non-unity Lewis number flames in LES. Combust. Sci. Technol. **186**, 1338–1369 (2014a)

Katragadda, M., Malkeson, S.P., Chakraborty, N.: Modelling of the curvature term of the flame surface density transport equation in the context of Reynolds averaged Navier Stokes simulation. Int. J. Spray Dyn. Combust. **6**(2), 163–198 (2014b)

Keil, F.B., Chakraborty, N., Klein, M.: Flame surface density transport statistics for high pressure turbulent premixed Bunsen Flames in the context of Large Eddy simulation. Combust. Sci. Technol. **192**, 2070–2092 (2020)

Keil, F.B., Amzehnhoff, M., Ahmed, U., Chakraborty, N., Klein, M.: Comparison of flame propagation statistics extracted from DNS based on simple and detailed chemistry part 1: fundamental flame turbulence interaction. Energies **14**, 5548 (2021a)

Keil, F.B., Amzehnhoff, M., Ahmed, U., Chakraborty, N., Klein, M.: Comparison of flame propagation statistics extracted from DNS based on simple and detailed chemistry part 2: influence of choice of reaction progress variable. Energies **14**, 5695 (2021b)

Keppeler, R., Tangermann, E., Allaudin, U., Pfitzner, M.: LES of low to high turbulent combustion in an elevated pressure environment. Flow Turb. Combust. **92**, 767–802 (2014)

Kim, J., Satija, A., Lucht, R.P., Gore, J.P.: Effects of turbulent flow regime on perforated plate stabilized piloted lean premixed flames. Combust. Flame **211**, 158–172 (2020)

Klein, M., Chakraborty, N., Pfitzner, M.: Analysis of the combined modelling of subgrid transport and filtered flame propagation for premixed turbulent combustion. Flow Turb. Combust. **96**, 921–938 (2016)

Klein, M., Chakraborty, N., Ketterl, S.: A comparison of strategies for direct numerical simulation of turbulence chemistry interaction in generic planar turbulent premixed flames. Flow Turb. Combust **199**, 955–971 (2017)

Knikker, R., Veynante, D., Meneveau, C.: A priori testing of a similarity model for large eddy simulations of turbulent premixed combustion. Proc. Combust. Inst. **29**, 2105–2111 (2002)

Luca, S., Attili, A., Lo Schiavo, E., Creta, F., Bisetti, F.: On the statistics of flame stretch in turbulent premixed jet flames in the thin reaction zone regime at varying Reynolds number. Proc. Combust. Inst. **37**, 2451–2459 (2019)

Ma, T., Stein, O.T., Chakraborty, N., Kempf, A.M.: A posteriori testing of algebraic flame surface density models for LES. Combust. Theor. Modell. **17**, 431–482 (2013)

Ma, T., Stein, O.T., Chakraborty, N., Kempf, A.M.: A-posteriori testing of the flame surface density transport equation for LES. Combust. Theory Modell. **18**, 32–64 (2014)

Meneveau, C., Poinsot, T.: Stretching and quenching of flamelets in premixed turbulent combustion. Combust. Flame **86**, 311–332 (1991)

Papapostolou, V., Chakraborty, N., Klein, M., Im, H.G.: Effects of reaction progress variable definition on the flame surface density transport statistics and closure for different combustion regimes. Combust. Sci. Technol. **191**, 1276–1293 (2019)

Peters, N., Terhoeven, P., Chen, J.H., Echekki, T.: Statistics of flame displacement speeds from computations of 2-D unsteady methane-Air flames. Proc. Combust. Inst. **27**, 833–839 (1998)

Peters, N.: Turbulent Combustion, 1st edn. Cambridge University Press, Cambridge (2000)

Poinsot, T., Lele, S.K.: Boundary conditions for direct simulation of compressible viscous flows. J. Comp. Phys. **101**, 104–129 (1992)

Poinsot, T., Veynante, D.: Theoretical and Numerical Combustion. R.T. Edwards Inc., Philadelphia (2001)

Pope, S.B.: The evolution of surfaces in turbulence. Int. J. Eng. Sci. **26**(5), 445–469 (1988)

Rasool, R., Klein, M., Chakraborty, N.: Flame surface density based mean reaction rate closure for Reynolds averaged Navier Stokes methodology in turbulent premixed Bunsen Flames with non-unity Lewis number. Combust. Flame (2022). https://doi.org/10.1016/j.combustflame.2021.111766

Reddy, H., Abraham, J.: Two-dimensional direct numerical simulation evaluation of the flame surface density model for flames developing from an ignition kernel in lean methane/air mixtures under engine conditions. Phys. Fluids **24**, 105108 (2012)

Rogallo, R.S.: Numerical experiments in homogeneous turbulence, NASA Technicla Memorandum 81315, NASA AMES Research Centre, California (1981)

Sabelnikov, V., Lipatnikov, A.N., Chakraborty, N., Nishiki, S., Hasagawa, T.: A balance equation for the mean rate of product creation in premixed turbulent flames. Proc. Combust. Inst. **36**, 1893–1901 (2017)

Sellmann, J., Lai, J., Chakraborty, N., Kempf, A.M.: Flame surface density based modelling of head-on quenching of turbulent premixed flames. Proc. Combust. Inst. **36**, 1817–1825 (2017)

Song, W., Hernandez-Perez, F.E., Tingas, E., Im, H.G.: Statistics of local and global flame speed and structure for highly turbulent H_2/air premixed flames. Combust. Flame **232**, 111513 (2021)

Song, W., Hernandez-Perez, F.E., Tingas, E., Im, H.G.: Diffusive effects of hydrogen on pressurized lean turbulent hydrogen-air premixed flames. Combust. Flame **246**, 112423 (2022)

Sreenivasan, K.R.: On the scaling of the turbulence energy dissipation rate. Phys. Fluids **27**, 1048 (1984)

Tamadonfar, P., Gülder, Ö.L.: Flame brush characteristics and burning velocities of premixed turbulent methane/air Bunsen flames. Combust. Flame **161**, 3154–3165 (2014)

Trivedi, S., Cant, R.S.: Turbulence intensity and length scale effects on premixed turbulent flame propagation. Flow Turb. Combust. **109**, 101–123 (2022)

Trouvé, A., Poinsot, T.: The evolution equation for flame surface density in turbulent premixed combustion. J. Fluid Mech. **278**, 1–31 (1994)

Varma, A.R., Ahmed, U., Klein, M., Chakraborty, N.: Effects of turbulent length scale on the bending effect of turbulent burning velocity in premixed turbulent combustion. Combust. Flame **233**, 111569 (2021)

Varma, A., Ahmed, U., Chakraborty, N.: Effects of body forces on the statistics of flame surface density and its evolution in statistically planar turbulent premixed flames. Flow Turb. Combust. **108**, 181–212 (2022a)

Varma, A.R., Ahmed, U., Chakraborty, N.: Effects of buoyancy on turbulent scalar flux closure for turbulent premixed flames in the context of Reynolds averaged Navier Stokes simulations. Combust. Theor. Modell. (2022b). https://doi.org/10.1080/13647830.2022.2049881

Veynante, D., Piana, J., Duclos, J.M., Martel, C.: Experimental analysis of flame surface density models for premixed turbulent combustion. Proc. Combust. Inst. **26**, 413–420 (1996)

Veynante, D., Trouvé, A., Bray, K.N.C., Mantel, T.: Gradient and counter-gradient scalar transport in turbulent premixed flames. J. Fluid Mech. **32**, 63–293 (1997)

Weller, H.G., Tabor, G., Gosman, A.D., Fureby, C.: Application of flame wrinkling LES combustion model to a turbulent mixing layer. Proc. Combust. Inst. **27**, 899–907 (1998)

Wray, A.A.: Minimal Storage Time Advancement Schemes for Spectral Methods, Unpublished Report. NASA Ames Research Center, California (1990)

Yu, R., Lipatnikov, A.N.: DNS study of dependence of bulk consumption velocity in a constant-density reacting flow on turbulence and mixture characteristics. Phys. Fluids **29**, 065116 (2017)